mRNA vaccine-elicited antibodies to SARS-CoV-2 and circulating variants

Zijun Wang[1,*], Fabian Schmidt[2,*], Yiska Weisblum[2,*], Frauke Muecksch[2,*], Christopher O. Barnes[3,*], Shlomo Finkin[1,*], Dennis Schaefer-Babajew[1,*], Melissa Cipolla[1*], Christian Gaebler[1*], Jenna A. Lieberman[4,*], Thiago Y. Oliveira[1], Zhi Yang[3], Morgan E. Abernathy[3], Kathryn E. Huey-Tubman[3], Arlene Hurley[5], Martina Turroja[1], Kamille A. West[6], Kristie Gordon[1], Katrina G. Millard[1], Victor Ramos[1], Justin Da Silva[2], Jianliang Xu[4], Robert A. Colbert[7], Roshni Patel[1], Juan Dizon[1], Cecille Unson-O'Brien[1], Irina Shimeliovich[1], Anna Gazumyan[1], Marina Caskey[1], Pamela J. Bjorkman[3,#], Rafael Casellas[4,8,#], Theodora Hatziioannou[2,#], Paul D. Bieniasz[2,9,#], Michel C. Nussenzweig[1,9,#]

[1]Laboratory of Molecular Immunology, The Rockefeller University, New York, NY 10065, USA.

[2]Laboratory of Retrovirology, The Rockefeller University, New York, NY 10065, USA.

[3] Division of Biology and Biological Engineering, California Institute of Technology, Pasadena, CA, USA.

[4]Lymphocyte Nuclear Biology, National Institute of Arthritis and Musculoskeletal and Skin Diseases, National Institutes of Health, Bethesda, MD 20892.

[5]Hospital Program Direction, The Rockefeller University, New York, NY 10065, USA.

[6]Department of Transfusion Medicine, National Institutes of Health Clinical Center, Bethesda, MD 20892.

[7]Pediatric Translational Research Branch and Office of the Clinical Director, National Institute of Arthritis and Musculoskeletal and Skin Diseases, National Institutes of Health, Bethesda, MD 20892.

[8]The NIH Regulome Project, National Institutes of Health, Bethesda, MD 20892.

[9] Howard Hughes Medical Institute

[*]Equal contribution

[#]Send correspondence to Paul Bieniasz: pbieniasz@rockefeller.edu; Pamela Bjorkman: bjorkman@caltech.edu; Rafael Casellas: rafael.casellas@nih,gov; Theodora Hatziioannou: thatziio@rockefeller.edu; Michel C. Nussenzweig: nussen@rockefeller.edu

To date severe acute respiratory syndrome coronavirus-2 (SARS-CoV-2) has infected over 100 million individuals resulting in over two million deaths. Many vaccines are being deployed to prevent coronavirus disease 2019 (COVID-19) including two novel mRNA-based vaccines[1,2]. These vaccines elicit neutralizing antibodies and appear to be safe and effective, but the precise nature of the elicited antibodies is not known[3-6]. Here we report on the antibody and memory B cell responses in a cohort of 20 volunteers who received either the Moderna (mRNA-1273) or Pfizer-BioNTech (BNT162b2) vaccines. Consistent with prior reports, 8 weeks after the second vaccine injection volunteers showed high levels of IgM, and IgG anti-SARS-CoV-2 spike protein (S) and receptor binding domain (RBD) binding titers[3,5,6]. Moreover, the plasma neutralizing activity, and the relative numbers of RBD-specific memory B cells were equivalent to individuals who recovered from natural infection[7,8]. However, activity against SARS-CoV-2 variants encoding E484K or N501Y or the K417N:E484K:N501Y combination was reduced by a small but significant margin. Consistent with these findings, vaccine-elicited monoclonal antibodies (mAbs) potently neutralize SARS-CoV-2, targeting a number of different RBD epitopes in common with mAbs isolated from infected donors. Structural analyses of mAbs complexed with S trimer suggest that vaccine- and virus-encoded S adopts similar conformations to induce equivalent anti-RBD antibodies. However, neutralization by 14 of the 17 most potent mAbs tested was reduced or abolished by either K417N, or E484K, or N501Y mutations. Notably, the same mutations were selected when recombinant vesicular stomatitis virus (rVSV)/SARS-CoV-2 S was cultured in the presence of the vaccine elicited mAbs. Taken together the results suggest that the monoclonal antibodies in clinical use should be tested

59 **against newly arising variants, and that mRNA vaccines may need to be updated**

60 **periodically to avoid potential loss of clinical efficacy.**

61 Between 19 October 2020 and 15 January 2021, 20 volunteers who received two doses of the
62 Moderna (n=14) or Pfizer-BioNTech mRNA (n=6) vaccines were recruited for blood donation
63 and analyzed. Ages of the analyzed volunteers ranged from 29-69 years (median 43); 12
64 (60%) were male and 8 (40%) female. 16 participants identified as Caucasian, 2 as Hispanic, and
65 1 as African American or Asian, respectively. The time from the second vaccination to sample
66 collection varied between 3-14 weeks with an average of 8 weeks. None of the volunteers had a
67 history of prior SARS-CoV-2 infection and none experienced serious adverse events after
68 vaccination (Extended Data Table 1).
69
70 **Vaccine plasma binding and neutralizing activity against SARS-CoV-2**
71 Plasma IgM, IgG and IgA responses to SARS-CoV-2 S and RBD were measured by enzyme-
72 linked immunosorbent assay (ELISA)[7,8]. All individuals tested showed reactivity to S and RBD
73 that was significantly higher compared to pre-COVID-19 historic controls (Extended Data Fig
74 1a-f). As might be expected anti-S and -RBD IgG levels were higher than IgM or IgA.
75 Moreover, there was a strong positive correlation between anti-RBD and anti-S response in all
76 three immunoglobulin isotypes measured (Extended Data Fig 1g-i). In line with previous
77 reports[3,6,9], IgG and IgM levels were significantly higher in the vaccinated group compared to a
78 cohort of convalescent patients assayed 1.3 and 6.2 months after infection, while IgA levels were
79 similar (Extended Data Fig 1j-l).
80
81 Plasma neutralizing activity was determined using human immunodeficiency virus-1 (HIV-1)
82 pseudotyped with SARS-CoV-2 S protein[7,8,10]. In agreement with previous reports[3,6,9], there was
83 a broad range of plasma neutralizing activity 3-14 weeks after the second vaccine dose that was

84 similar to that elicited by natural infection in a convalescent cohort after 1.3 months, and greater
85 than the activity at 6.2 months after infection (Fig. 1a, Extended Data Table 1). There was no
86 significant difference in neutralizing activity between the Moderna and Pfizer-BioNTech
87 vaccines (Fig. 1b). Whereas convalescent antibody titers tend to correlate with severity and
88 length of time of infection, additional sampling would be required to understand the correlates of
89 the magnitude of the vaccine responses. As expected, plasma neutralizing activity was directly
90 correlated to anti-S and -RBD binding titers in ELISAs[7,8] (Fig. 1c, d, and Extended Data Fig. 2a-
91 d). Finally, RBD and S binding, and neutralizing activities were directly correlated to the time
92 between the first vaccine dose and blood donation with significantly reduced levels in all 3
93 measurements with time (Fig. 1e, f and g, and Extended Data Fig. 2e-h)[11]. However, this and
94 other small studies[3,11] cannot accurately predict the half-life of the neutralizing response. Larger
95 numbers of individuals in diverse cohorts will need to be studied to determine the precise half-
96 life of the vaccine elicited neutralizing response.
97
98 To determine whether plasma from vaccinated individuals can neutralize circulating SARS-CoV-
99 2 variants of concern and mutants that arise *in vitro* under antibody pressure [12,13], we tested
100 vaccinee plasma against a panel of 10 mutant pseudotype viruses including recently reported
101 N501Y (B1.1.7 variant), K417N, E484K and the combination of these 3 RBD mutations
102 (501Y.V2 variant)[14-19]. Vaccinee plasma was significantly less effective in neutralizing the HIV-
103 1 virus pseudotyped with certain SARS-CoV-2 mutant S proteins (Fig. 1h and i and Extended
104 Data Fig. 2j). Among the volunteer plasmas tested there was a 1- to 3-fold decrease in
105 neutralizing activity against E484K, N501Y and the K417N:E484K:N501Y combination (p=
106 0.0033, p=0.0002, and p<0.0001, respectively, Fig. 1h and i). Similarly, convalescent plasma

107 obtained 1.3 and 6.2 months after infection was 0.5- to 29- and 0.5- to 20.2-fold less effective in
108 neutralizing the K417N:E484K:N501Y combination ($p=0.001$ and $p<0.0001$, respectively, Fig.
109 1j, Extended Data Table 2). We conclude that the plasma neutralizing activity elicited by either
110 mRNA vaccination or natural infection is variably but significantly less effective against
111 pseudoviruses that carry RBD mutations found in emerging SARS-CoV-2 variants.
112
113 **Vaccine-elicited SARS-CoV-2 RBD-specific monoclonal antibodies**
114 Although circulating antibodies derived from plasma cells wane over time, long-lived immune
115 memory can persist in expanded clones of memory B cells[7,20]. We used flow cytometry to
116 enumerate the circulating SARS-CoV-2 RBD-specific memory B cells elicited by mRNA
117 immunization[7,8] (Fig. 2a, Extended Data Fig. 3a and b). We focused on the RBD since it is the
118 target of the majority of the more potent SARS-CoV-2 neutralizing antibodies discovered to
119 date[21-26]. Notably, the percentage of RBD-binding memory B cells in vaccinees was significantly
120 greater than in naturally infected individuals assayed after 1.3 months, but similar to the same
121 individuals assayed after 6.2 months (Fig. 2b). The percentage of RBD-binding memory B cells
122 in vaccinees was not correlated to the time after vaccination (Extended Data Fig. 3c). Thus,
123 mRNA vaccination elicits a robust SARS-CoV-2 RBD-specific B cell memory response that
124 resembles natural infection.
125
126 To examine the nature of the antibodies produced by memory B cells in response to vaccination,
127 we obtained 1,409 paired antibody heavy and light chains from RBD binding single B cells from
128 14 individuals (n=10 Moderna and n=4 Pfizer-BioNTech vaccinees) (Extended Data Table 3).
129 Expanded clones of cells comprised 4-50% of the overall RBD binding memory B cell

130 compartment (Fig. 2c and d, and Extended Data Fig. 3d). Similar to natural infection, IGVH 3-
131 53, and 3-30 and some IGVL genes were significantly over-represented in the RBD-binding
132 memory B cell compartment of vaccinated individuals (Fig. 2e, Extended Data Fig. 4a). In
133 addition, antibodies that share the same combination of IGHV and IGLV genes in vaccinees
134 comprised 39% of all the clonal sequences (Extended Data Fig. 4b) and 59% when combined
135 with naturally infected individuals[7,8] (Fig. 2f), and some of these antibodies were nearly identical
136 (Extended Data Table 3 and 4). The number of V gene nucleotide mutations in vaccinees is
137 greater than in naturally infected individuals assayed after 1.3 months, but lower than that in the
138 same individuals assayed after 6.2 months (Fig. 2g and Extended Data Fig. 5a). The length of the
139 IgH CDR3 was similar in both natural infected individuals and vaccinees and hydrophobicity
140 was below average[27] (Fig. 2h and Extended Data Fig. 5a and b). Thus, the IgG memory response
141 is similar in individuals receiving the Pfizer-BioNTech and Moderna vaccines and both are rich
142 in recurrent and clonally expanded antibody sequences.
143
144 One hundred and twenty-seven representative antibodies from 8 individuals were expressed and
145 tested for reactivity to the RBD (Extended Data Table 5). The antibodies included: (1) 76 that
146 were randomly selected from those that appeared only once, and (2) 51 representatives of
147 expanded clones. Of the antibodies tested 98% (124 out of the 127) bound to RBD indicating
148 that single cell sorting by flow cytometry efficiently identified B cells producing anti-RBD
149 antibodies (Extended Data Fig. 6a-c and Table 5). In anti-RBD ELISAs the mean half-maximal
150 effective concentration (EC_{50}) was higher than that observed in infected individuals after 6.2
151 months but not significantly different from antibodies obtained 1.3 months after infection
152 (Extended Data Fig. 6a, and Table 5 and [7,8]). To examine memory B cell antibodies for binding

153 to circulating SARS-CoV-2 variants and antibody resistant mutants we performed ELISAs using
154 mutant RBDs[12,15,28-31]. Twenty-two (26%) of the 84 antibodies tested showed at least 5-fold
155 decreased binding to at least one of the mutant RBDs (Extended data Fig. 6d-n and Table 5).
156
157 SARS-CoV-2 S pseudotyped viruses were used to measure the neutralizing activity of all 127
158 antibodies[7,8,10] (Fig. 3a, Extended Data Table 5). Consistent with the plasma neutralization
159 results, the geometric mean neutralization half-maximal inhibitory concentration of the Pfizer-
160 BioNTech and Moderna vaccinee antibodies were not significantly different from each other or
161 to antibody collections obtained from naturally infected individuals 1.3 or 6.2 months after
162 infection (Fig. 3a and [7,8]).
163
164 To examine the neutralizing breadth of the monoclonal antibodies and begin to map their target
165 epitopes we tested 17 of the most potent antibodies (Extended data Table 6), 8 of which carried
166 IgHV3-53, against a panel of 12 SARS-CoV-2 variants: A475V is resistant to class 1 antibodies
167 (structurally defined as described[29]); E484K and Q493R are resistant to class 2
168 antibodies[7,8,12,13,29,30,32,33]; while R346S, N439K, and N440K are resistant to class 3
169 antibodies[7,8,12,13,29,33]. Additionally, K417N, Y453F, S477R, N501Y, and D614G represent
170 circulating variants some of which have been associated with rapidly increasing case
171 numbers[14,15,19,33-35]. Based on their neutralizing activity against the variants, all but 3 of the
172 antibodies were provisionally assigned to a defined antibody class or a combination (Fig. 3b). As
173 seen in natural infection, a majority of the antibodies tested (9/17) were at least ten-fold less
174 effective against pseudotyped viruses carrying the E484K mutation[7,12,29]. In addition, 5 of the
175 antibodies were less potent against K417N and 4 against N501Y by ten-fold or more (Fig. 3b).

176 Similar results were obtained with antibodies being developed for clinical use (REGN10987,
177 REGN10933, COV2-2196, COV2-2130, C135 and C144 (Extended data Fig. 7)). However,
178 antibody combinations remained effective against all of the variants tested confirming the
179 importance of using antibody combinations in the clinic (Extended data Fig. 7). Whether less
180 potent antibodies show similar degrees of sensitivity to these mutations remains to be
181 determined.
182
183 To determine whether antibody-imposed selection pressure could also drive the emergence of
184 resistance mutations *in vitro,* we cultured an rVSV/SARS-CoV-2 recombinant virus in the
185 presence of each of 18 neutralizing monoclonal antibodies. All of the tested antibodies selected
186 for RBD mutations. Moreover, in all cases the selected mutations corresponded to residues in the
187 binding sites of their presumptive antibody class (Fig. 3b and c). For example, antibody C627,
188 which was assigned to class 2 based on sensitivity to the E484K mutation, selected for the
189 emergence of the E484K mutation *in vitro* (Fig 3c). Notably, 6 of the antibodies selected for
190 K417N, E or T, 5 selected for E484K and 3 selected for N501Y, T or H, which coincide with
191 mutations present in the circulating B.1.1.17/501Y.V1, B.1.351/501Y.V2 and B1.1.28/501.V3
192 (P.1) variants that have been associated with rapidly increasing case numbers in particular
193 locales[14,17,18,36].
194
195 **Cryo-EM Mapping of Antibody Epitopes**
196 To further characterize antibody epitopes and mechanisms of neutralization, we characterized
197 seven complexes between mAb Fab fragments and the prefusion, stabilized ectodomain trimer of
198 SARS-CoV-2 S glycoprotein[37] using single-particle cryo-EM (Fig 4 and Extended Data Table 7).

199 Overall resolutions ranged from 5-8 Å (Extended Data Fig. 8) and coordinates from S trimer and
200 representative Fab crystal structures were fit by rigid body docking into the cryo-EM density
201 maps to provide a general assessment of antibody footprints/RBD epitopes. Fab-S complexes
202 exhibited multiple RBD-binding orientations recognizing either 'up'/'down' (Fig 4a-j) or solely
203 'up' (Fig 4k-n) RBD conformations, consistent with structurally defined antibody classes from
204 natural infection (Fig 4o)[29]. The majority of mAbs characterized (6 of 7) recognized epitopes that
205 included RBD residues involved in ACE2 recognition, suggesting a neutralization mechanism
206 that directly blocks ACE2-RBD interactions. Additionally, structurally defined antibody epitopes
207 were consistent with RBD positions that were selected in rVSV/SARS-CoV-2 recombinant virus
208 outgrowth experiments, including residues K417, N439/N440, E484, and N501 (Fig 3c and Fig
209 4f-j,m,n). Taken together, these data suggest that functionally similar antibodies are raised during
210 vaccination and natural infection, and that the RBDs of spike trimers translated from the mRNA
211 delivered by vaccination adopt both 'up' and 'down' conformations as observed on structures of
212 trimer ectodomains[29] and trimers on the surface of SARS-CoV-2 virions[38].
213
214 **Discussion**
215 The mRNA-based SARS-CoV-2 vaccines are safe and effective and being deployed globally to
216 prevent infection and disease. The vaccines elicit antibody responses against the RBD, the major
217 target of neutralizing antibodies[21-26], in a manner that resembles natural infection. Notably, the
218 neutralizing antibodies produced by mRNA vaccination target the same epitopes as natural
219 infection. The data are consistent with SARS-CoV-2 spike trimers translated from the injected
220 RNA adopting a range of different conformations. Moreover, different individuals immunized
221 with either the Moderna (mRNA-1273) or Pfizer-BioNTech (BNT162b2) vaccines produce

222 closely related and nearly identical antibodies. Whether or not neutralizing antibodies to epitopes
223 other that RBD are elicited by vaccination remains to be determined.
224
225 Human neutralizing monoclonal antibodies to the SARS-CoV-2 RBD can be categorized as
226 belonging to 4 different classes based on their target regions on the RBD[29]. Class 1 and 2
227 antibodies are among the most potent and also the most abundant antibodies[7,8,21,22,25,39]. These
228 antibodies target epitopes that overlap or are closely associated with RBD residues K417, E484
229 and N501. They are frequently sensitive to mutation in these residues and select for K417N,
230 E484K and N501Y mutations in SARS-CoV-2 S protein expression libraries in yeast and VSV
231 [12,15,33]. To avert selection and escape, antibody therapies should be composed of combinations of
232 antibodies that target non-overlapping or highly conserved epitopes[8,12,13,33,40-44].
233
234 A number of circulating SARS-CoV-2 variants that have been associated with rapidly increasing
235 case numbers and have particular prevalence in the UK (B.1.1.7/501Y.V1), South Africa
236 (B.1.351/501Y.V2) and Brazil (P.1)[14,17,18,36]. Our experiments indicate that the RBD mutations
237 found in these variants, and potentially others that carry K417N/T, E484K and N501Y
238 mutations, can reduce the neutralization potency of vaccinee and convalescent plasma against
239 SARS-CoV-2 pseudotyped viruses. Although our assays are limited to pseudotyped viruses there
240 is an excellent correlation between pseudotyped and authentic SARS-CoV-2 neutralization
241 assays[10]. In addition, similar results have been reported by others using vaccinee and
242 convalescent plasmas and a variety of different pseudotype and authentic virus assays[15,31,45-49].
243

244 The comparatively modest effects of the mutations on viral sensitivity to plasma reflects the
245 polyclonal nature of the neutralizing antibodies in vaccinee plasma. Nevertheless, emergence of
246 these particular variants is consistent with the dominance of the class 1 and 2 antibody response
247 in infected or vaccinated individuals. We speculate that these mutations emerged in response to
248 immune selection in individuals with non-sterilizing immunity. What the long-term effect of
249 accumulation of mutations on the SARS-CoV-2 pandemic will be is not known, but the common
250 cold coronavirus HCoV-229E evolves antigenic variants that are comparatively resistant to the
251 older sera but remain sensitive to contemporaneous sera[50]. Thus, it is possible that these
252 mutations and others that emerge in individuals with suboptimal or waning immunity will erode
253 the effectiveness of natural and vaccine elicited immunity. The data suggests that SARS-CoV-2
254 vaccines and antibody therapies may need to be updated and immunity monitored in order to
255 compensate for viral evolution.
256

257 **Figure Legends**

258 **Fig. 1. Plasma neutralizing activity.**

259 **a,** SARS-CoV-2 pseudovirus neutralization assay. NT_{50} values for COVID-19 convalescent
260 plasma measured at 1.3 months[8] and 6.2 months[7] after infection as well as plasma from
261 vaccinees. NT_{50} values lower than 10 were plotted at 10. Mean of 2 independent experiments.
262 Red bars and indicated values represent geometric mean NT_{50} values. Statistical significance was
263 determined using the two-tailed Mann-Whitney U-test. Pre-COVID-19 historical control plasma
264 was analyzed as a negative control and showed no detectable neutralization (NT_{50}<10). **b**, NT_{50}
265 values for Moderna mRNA-1273 (black) and Pfizer-BioNTech BNT162b2 (red) vaccine
266 recipients. Red bars and indicated values represent geometric mean NT_{50} values. Statistical
267 significance was determined using the two-tailed Mann-Whitney U-test. **c**, Anti-RBD IgG AUC
268 (Y axis) plotted against NT_{50} (X axis) r=0.82, p<0.0001. **d,** Anti-S IgG AUC (Y axis) plotted
269 against NT_{50} (X axis) r=0.83, p<0.0001. **e**, Anti-RBD IgG AUC (Y axis) plotted against time
270 between first dose and blood draw (X axis) r=-0.59 p=0.0058. **f**, Anti-S IgG AUC (Y axis)
271 plotted against time between first dose and blood draw (X axis) r=-0.62 p=0.0038. **g**, NT_{50} (Y
272 axis) plotted against time between first dose and blood draw (X axis) r=-0.69 p=0.0008. The r
273 and p values for correlations in **c-g** were determined by two-tailed Spearman correlation.
274 Moderna vaccinees are in black and Pfizer-BioNTech in red. **h.** Examples of neutralization
275 assays, comparing the sensitivity of pseudotyped viruses with WT and RBD mutant SARS-CoV-
276 2 S proteins to vaccinee plasma. MOD1 and PFZ10 indicate two representative individuals
277 receiving the Moderna and Pfizer-BioNTech vaccine, respectively (for details see Ext. Data
278 Table 1). **i,** NT50 values for vaccinee plasma (n=15) neutralization of pseudotyped viruses with
279 WT and the indicated RBD-mutant SARS-CoV-2 S proteins. Pfizer-BioNTech vaccinees in red.

280 **j**, NT50 values for convalescent plasma (n=45) neutralization of pseudotyped viruses with WT
281 and KEN (K417N/E484K/N501Y) SARS-CoV-2 S proteins. Statistical significance in **i** and **j**
282 was determined using one tailed t-test. All experiments were performed a minimum of 2 times.
283 Pseutotyped viruses containing the E484K mutation and corresponding WT controls contain the
284 R683G mutation (for details see methods).
285
286 **Fig. 2. Memory B cell antibodies.**
287 **a**, Representative flow cytometry plots showing dual AlexaFluor-647-RBD and PE-RBD binding
288 B cells for 4 vaccinees. **b,** as in **a,** dot plot summarizes the percentage of RBD binding B cells in
289 19 vaccinees, in comparison to a cohort of infected individuals assayed 1.3 and 6.2 months after
290 infection[7,8]. Individuals who received the Moderna vaccine are shown in black and Pfizer-
291 BioNTech vaccine recipients in red. Red horizontal bars indicate mean values. Statistical
292 significance was determined using two-tailed Mann–Whitney U-tests. **c,** Pie charts show the
293 distribution of antibody sequences from the 4 individuals in **a.** The number in the inner circle
294 indicates the number of sequences analyzed. Pie slice size is proportional to the number of
295 clonally related sequences. The black outline indicates the frequency of clonally expanded
296 sequences. **d,** as in **c,** graph shows relative clonality among 14 vaccinees assayed, individuals
297 who received the Moderna vaccine are shown in black and Pfizer-BioNTech vaccine recipients
298 in red. Red horizontal bars indicate mean values. Statistical significance was determined using
299 two-tailed Mann–Whitney U-tests. **e,** Graph shows relative abundance of human IGVH genes
300 Sequence Read Archive accession SRP010970 (orange), and vaccinees (blue). A two-sided
301 binomial test was used to compare the frequency distributions, significant differences are
302 denoted with stars (* $p < 0.05$, ** $p < 0.01$, *** $p < 0.001$, **** = $p < 0.0001$). **f,** Clonal

303 relationships between sequences from 14 vaccinated individuals (Moderna in black, Pfizer-
304 BioNTech in red Extended Data Table 3) and naturally infected individuals (in green, from[7,8]).
305 Interconnecting lines indicate the relationship between antibodies that share V and J gene
306 segment sequences at both IGH and IGL. Purple, green and grey lines connect related clones,
307 clones and singles, and singles to each other, respectively. **g,** Number of somatic nucleotide
308 mutations in the IGVH (top) and IGVL (bottom) in vaccinee antibodies (Extended Data Table 3)
309 compared to natural infection obtained 1.3 or 6.2 months after infection[7,8]. Statistical
310 significance was determined using the two-tailed Mann–Whitney U-tests and red horizontal bars
311 indicate mean values. **h,** as in **g,** but for CDR3 length.
312
313 **Fig. 3: Anti-SARS-CoV-2 RBD monoclonal antibody neutralizing activity.**
314 **a,** SARS-CoV-2 pseudovirus neutralization assay. IC_{50} values for antibodies cloned from
315 COVID-19 convalescent patients measured at 1.3 and 6.2 months[7,8] after infection as well as
316 antibodies cloned from Moderna mRNA-1273 (black) and Pfizer-BioNTech BNT162b2 (red)
317 mRNA- vaccine recipients. Antibodies with IC_{50} values above 1000 ng/ml were plotted at 1000
318 ng/ml. Mean of 2 independent experiments. Red bars and indicated values represent geometric
319 mean IC_{50} values in ng/ml. Statistical significance was determined using the two-tailed Mann-
320 Whitney U-test. Isotype control antibody was analyzed in parallel and showed no detectable
321 neutralization. **b,** IC_{50} values for 17 selected mAbs for neutralization of wild type and the
322 indicated mutant SARS-CoV-2 pseudoviruses. Color gradient indicates IC_{50} values ranging from
323 0 (white) to 1000 ng/ml (red). **c**, Antibody selection pressure can drive emergence of S variants
324 in cell culture; the percentage of sequence reads encoding the indicated RBD mutations after a
325 single passage of rVSV/SARS-CoV-2 in the presence of the indicated antibodies is tabulated.

326 Color gradient indicates percentage of sequence reads bearing the indicated mutation ranging
327 from 0 (white) to 100 (red). Positions for which no sequence read was detected are shown in
328 grey. The percentages calculated for a given position are based on all the reads, and not just the
329 reads that include that position. K417N, E484K/R683G and N501 are highlighted in **b** and **c** as
330 they constitute important circulating variants.
331
332 **Fig. 4. Cryo-EM reconstructions of Fab-S complexes.**
333 Cryo-EM densities for Fab-S complexes (**a-e**; **k-l**) and close-up views of antibody footprints on
334 RBDs (**f-j**; **m-n**) are shown for neutralizing mAbs. As expected, due to Fab inter-domain
335 flexibility, cryo-EM densities (**a-e**; **k-l**) were weak for the Fab C_H-C_L domains. Models of
336 antibody footprints on RBDs (**f-j**; **m-n**) are presented as Fab V_H-V_L domains (cartoon)
337 complexed with the RBD (surface). To generate models, coordinates of stabilized S trimer (PDB
338 6XKL) and representative Fab fragments (PDB 6XCA or 7K8P) with CDR3 loops removed were
339 fit by rigid body docking into the cryo-EM density maps. **a,f,** C669; **b,g,** C643; **c,h,** C603; **d,i,**
340 C601; **e,j,** C670; **k,m,** C666; and **l,n,** C663. RBD residues K417, N439, N440, E484, and N501
341 are highlighted as red surfaces. The N343 glycan is shown as a teal sphere. **o,** Composite model
342 illustrating targeted epitopes of RBD-specific neutralizing mAbs (shown as V_H-V_L domains in
343 colors from panels **a-l**) elicited from mRNA vaccines.
344

345

346 **Data reporting**

347 No statistical methods were used to predetermine sample size. The experiments were not
348 randomized and the investigators were not blinded to allocation during experiments and outcome
349 assessment.

350

351 **Study participants**.

352 To isolate and characterize anti-SARS-CoV-2 RBD antibodies from vaccinees, a cohort
353 of 20 individuals that participated in either the Moderna or Pfizer-BioNTech phase 3 vaccine
354 clinical trials and did not report prior history of SARS-CoV-2 infection was recruited at the NIH
355 Blood Center and the Rockefeller University Hospital for blood donation. Eligible participants
356 included adults, at least 18 years of age with no known heart, lung, kidney disease or bleeding
357 disorders, no history of HIV-1 or malaria infection. All participants were asymptomatic at the
358 time of the study visit and had received a complete 2 dose regimen of either mRNA vaccine.
359 Informed consent was obtained from all participants and the study was conducted in accordance
360 with Good Clinical Practice. The study visits and blood draws were reviewed and approved
361 under the National Institutes of Health's Federalwide Assurance (FWA00005897), in accordance
362 with Federal regulations 45 CFR 46 and 21 CFR 5 by the NIH Intramural Research Program IRB
363 committee (IRB# 99CC0168, Collection and Distribution of Blood Components from Healthy
364 Donors for In Vitro Research Use) and by the Institutional Review Board of the Rockefeller
365 University (IRB# DRO-1006, Peripheral Blood of Coronavirus Survivors to Identify Virus-
366 Neutralizing Antibodies). For detailed participant characteristics see Extended Data Table 1.

367

368 **Blood samples processing and storage.**

369 Samples collected at NIH were drawn from participants at the study visit and processed within
370 24 hours. Briefly, whole blood samples were subjected to Ficoll gradient centrifugation after 1:1
371 dilution in PBS. Plasma and PBMC samples were obtained through phase separation of plasma
372 layer and Buffy coat phase, respectively. PBMCs were further prepared through centrifugation,
373 red blood cells lysis and washing steps, and stored in CellBanker cell freezing media
374 (Amsbio). All samples were aliquoted and stored at - 80 °C and shipped on dry ice. Prior to
375 experiments, aliquots of plasma samples were heat-inactivated (56°C for 1 hour) and then stored
376 at 4°C. Peripheral Blood Mononuclear Cells (PBMCs) obtained from samples collected at
377 Rockefeller University were purified as previously reported[7,8] by gradient centrifugation and
378 stored in liquid nitrogen in the presence of FCS and DMSO. Heparinized plasma samples were
379 aliquoted and stored at -20°C or less. Prior to experiments, aliquots of plasma samples were heat-
380 inactivated (56°C for 1 hour) and then stored at 4°C.

381

382 **ELISAs**

383 ELISAs[51,52] to evaluate antibodies binding to SARS-CoV-2 S (BioHub), RBD and additional
384 mutated RBDs were performed by coating of high-binding 96-half-well plates (Corning 3690)
385 with 50 µl per well of a 1µg/ml protein solution in PBS overnight at 4 °C. Plates were washed 6
386 times with washing buffer (1× PBS with 0.05% Tween-20 (Sigma-Aldrich)) and incubated with
387 170 µl per well blocking buffer (1× PBS with 2% BSA and 0.05% Tween-20 (Sigma)) for 1 h at
388 room temperature. Immediately after blocking, monoclonal antibodies or plasma samples were
389 added in PBS and incubated for 1 h at room temperature. Plasma samples were assayed at a
390 1:66.6 (RU samples) or a 1:33.3 (NIH samples) starting dilution and 7 additional threefold serial

391 dilutions. Monoclonal antibodies were tested at 10 µg/ml starting concentration and 10 additional
392 fourfold serial dilutions. Plates were washed 6 times with washing buffer and then incubated
393 with anti-human IgG, IgM or IgA secondary antibody conjugated to horseradish peroxidase
394 (HRP) (Jackson Immuno Research 109-036-088 109-035-129 and Sigma A0295) in blocking
395 buffer at a 1:5,000 dilution (IgM and IgG) or 1:3,000 dilution (IgA). Plates were developed by
396 addition of the HRP substrate, TMB (ThermoFisher) for 10 min (plasma samples) or 4 minutes
397 (monoclonal antibodies), then the developing reaction was stopped by adding 50 µl 1 M H_2SO_4
398 and absorbance was measured at 450 nm with an ELISA microplate reader (FluoStar Omega,
399 BMG Labtech) with Omega and Omega MARS software for analysis. For plasma samples, a
400 positive control (plasma from participant COV72[7,8], diluted 66.6-fold and with seven additional
401 threefold serial dilutions in PBS) was added to every assay plate for validation. The average of
402 its signal was used for normalization of all of the other values on the same plate with Excel
403 software before calculating the area under the curve using Prism V8.4 (GraphPad). For
404 monoclonal antibodies, the EC50 was determined using four-parameter nonlinear regression
405 (GraphPad Prism V8.4).
406
407 **Expression of RBD proteins**
408 Mammalian expression vectors encoding the RBDs of SARS-CoV-2 (GenBank MN985325.1; S
409 protein residues 319-539) and eight additional mutant RBD proteins (E484K, Q493R, R346S,
410 N493K, N440K, V367F, A475V, S477N and V483A) with an N-terminal human IL-2 or Mu
411 phosphatase signal peptide were previously described[30].
412
413 **Cells and viruses**

414 $293T_{Ace2}$ [8], 293T/ACE2.cl22 and HT1080/ACE2.cl14 cells[10] were cultured in Dulbecco's
415 Modified Eagle Medium (DMEM) supplemented with 10% fetal bovine serum (FBS) at 37°C
416 and 5% CO_2. Cells were periodically tested for contamination with mycoplasma or retroviruses.
417 rVSV/SARS-CoV-2/GFP chimeric virus stocks were generated by infecting 293T/ACE2.cl22
418 cells. Supernatant was harvested 1 day post infection (dpi), cleared of cellular debris, and stored
419 at -80°C. A plaque purified variant designated rVSV/SARS-CoV-2/GFP_{2E1} that encodes
420 D215G/R683G substitutions was used in these studies[10].
421
422 **Selection and analysis of antibody escape mutations**
423 For the selection of monoclonal antibody-resistant spike variants, an rVSV/SARS-CoV-2/GFP_{2E1}
424 (for details see[10]) population containing 10^6 infectious units was incubated with monoclonal
425 antibodies at 10-40 μg/ml for 1 hr at 37 °C. The virus-antibody mixtures were subsequently
426 incubated with 5×10^5 293T/ACE2cl.22 cells in 6-well plates. One day after infection the media
427 was replaced with fresh media containing the equivalent concentration of antibodies. Supernatant
428 was harvested 2 days after infection and 150 μl of the cleared supernatant was used to infect cells
429 for passage 2, while 150 μl was subjected to RNA extraction and sequencing.
430 For identification of putative antibody resistance mutations, RNA was extracted using
431 NucleoSpin 96 Virus Core Kit (Macherey-Nagel). The RNA was reversed transcribed using the
432 SuperScript VILO cDNA Synthesis Kit (Thermo Fisher Scientific). KOD Xtreme Hot Start DNA
433 Polymerase (Millipore Sigma) was used for amplification of cDNA using primers flanking the S-
434 encoding sequence. The PCR products were purified and sequenced as previously described[7,12].
435 Briefly, tagmentation reactions were performed using 1ul diluted cDNA, 0.25 μl Nextera TDE1
436 Tagment DNA enzyme (catalog no. 15027865), and 1.25 μl TD Tagment DNA buffer (catalog

437 no. 15027866; Illumina). Next, the DNA was ligated to unique i5/i7 barcoded primer
438 combinations using the Illumina Nextera XT Index Kit v2 and KAPA HiFi HotStart ReadyMix
439 (2X; KAPA Biosystems) and purified using AmPure Beads XP (Agencourt), after which the
440 samples were pooled into one library and subjected to paired-end sequencing using Illumina
441 MiSeq Nano 300 V2 cycle kits (Illumina) at a concentration of 12pM.
442 For analysis of the sequencing data, the raw paired-end reads were pre-processed to remove trim
443 adapter sequences and to remove low-quality reads (Phred quality score < 20) using BBDuk.
444 Reads were mapped to the rVSV/SARS-CoV-2/GFP sequence using Geneious Prime (Version
445 2020.1.2). Mutations were annotated using Geneious Prime, with a P-value cutoff of
446 10^{-6}. Because reads have randomly generated ends and different lengths, the mutations do not
447 necessarily have to occur on the same read. e.g K417N and N501Y might occur on the same read
448 or on different reads. The percentages calculated for position X are calculated based on all the
449 reads, and not just the reads, that include position X.
450
451 **SARS-CoV-2 pseudotyped reporter virus**
452 A panel of plasmids expressing RBD-mutant SARS-CoV-2 spike proteins in the context of
453 pSARS-CoV-2-$S_{\Delta 19}$ (based on (NC_045512)) have been described previously[12]. Additional
454 substitutions were introduced using either PCR primer-mediated mutagenesis or with synthetic
455 gene fragments (IDT) followed by Gibson assembly. The mutants E484K and KEN
456 (K417N+E484K+N501Y) were constructed in the context of a pSARS-CoV-2-$S_{\Delta 19}$ variant with
457 a mutation in the furin cleavage site (R683G). The NT50s and IC50 of these pseudotypes were
458 compared to a wildtype SARS-CoV-2 spike sequence carrying R683G in the subsequent
459 analyses, as appropriate.

460 Generation of SARS-CoV-2 pseudotyped HIV-1 particles was performed as previously
461 described[8]. Briefly, 293T cells were transfected with pNL4-3ΔEnv-nanoluc and pSARS-CoV-2-
462 $S_{\Delta 19}$ and pseudotyped virus stocks were harvested 48 hours after transfection, filtered and stored
463 at -80°C.
464
465 **SARS-CoV-2 pseudotype neutralization assays**
466 Plasma or monoclonal antibodies from vaccine recipients were four-fold or five-fold serially
467 diluted and then incubated with SARS-CoV-2 pseudotyped HIV-1 reporter virus for 1 h at 37 °C.
468 The antibody and pseudotyped virus mixture was added to $293T_{Ace2}$ cells[8] (for comparisons of
469 plasma or monoclonal antibodies from COVID-19-convalescents and vaccine recipients) or
470 HT1080ACE2.cl14 cells[10] (for analysis of spike mutants with vaccine recipient plasma or
471 monoclonal antibodies). After 48 h cells were washed with PBS and lysed with Luciferase Cell
472 Culture Lysis 5× reagent (Promega) and Nanoluc Luciferase activity in lysates was measured
473 using the Nano-Glo Luciferase Assay System (Promega) with the Glomax Navigator (Promega).
474 The relative luminescence units were normalized to those derived from cells infected with
475 SARS-CoV-2 pseudotyped virus in the absence of plasma or monoclonal antibodies. The half-
476 maximal and 80% or 90% neutralization titers for plasma (NT_{50} and NT_{80}/NT_{90}, respectively) or
477 half-maximal and 90% inhibitory concentrations for monoclonal antibodies (IC_{50} and IC_{90},
478 respectively) were determined using four-parameter nonlinear regression (least squares
479 regression method without weighting; constraints: top=1, bottom=0) (GraphPad Prism).
480
481 **Biotinylation of viral protein for use in flow cytometry**

482 Purified and Avi-tagged SARS-CoV-2 RBD was biotinylated using the Biotin-Protein Ligase-
483 BIRA kit according to manufacturer's instructions (Avidity) as described before[8]. Ovalbumin
484 (Sigma, A5503-1G) was biotinylated using the EZ-Link Sulfo-NHS-LC-Biotinylation kit
485 according to the manufacturer's instructions (Thermo Scientific). Biotinylated ovalbumin was
486 conjugated to streptavidin-BV711 (BD biosciences, 563262) and RBD to streptavidin-PE (BD
487 Biosciences, 554061) and streptavidin-AF647 (Biolegend, 405237)[8].
488
489 **Flow cytometry and single cell sorting**
490 Single-cell sorting by flow cytometry was performed as described previously[8]. Briefly,
491 peripheral blood mononuclear cells were enriched for B cells by negative selection using a pan-
492 B-cell isolation kit according to the manufacturer's instructions (Miltenyi Biotec, 130-101-638).
493 The enriched B cells were incubated in FACS buffer (1× PBS, 2% FCS, 1 mM EDTA) with the
494 following anti-human antibodies (all at 1:200 dilution): anti-CD20-PECy7 (BD Biosciences,
495 335793), anti-CD3-APC-eFluro 780 (Invitrogen, 47-0037-41), anti-CD8-APC-eFluor 780
496 (Invitrogen, 47-0086-42), anti-CD16-APC-eFluor 780 (Invitrogen, 47-0168-41), anti-CD14-
497 APC-eFluor 780 (Invitrogen, 47-0149-42), as well as Zombie NIR (BioLegend, 423105) and
498 fluorophore-labelled RBD and ovalbumin (Ova) for 30 min on ice. Single
499 CD3−CD8−CD14−CD16−CD20+Ova−RBD-PE+RBD-AF647+ B cells were sorted into
500 individual wells of 96-well plates containing 4 µl of lysis buffer (0.5× PBS, 10 mM DTT, 3,000
501 units/ml RNasin Ribonuclease Inhibitors (Promega, N2615) per well using a FACS Aria III and
502 FACSDiva software (Becton Dickinson) for acquisition and FlowJo for analysis. The sorted cells
503 were frozen on dry ice, and then stored at −80 °C or immediately used for subsequent RNA
504 reverse transcription.

505

506 **Antibody sequencing, cloning and expression**

507 Antibodies were identified and sequenced as described previously[8]. In brief, RNA from single
508 cells was reverse-transcribed (SuperScript III Reverse Transcriptase, Invitrogen, 18080-044) and
509 the cDNA stored at −20 °C or used for subsequent amplification of the variable IGH, IGL and
510 IGK genes by nested PCR and Sanger sequencing. Sequence analysis was performed using
511 MacVector. Amplicons from the first PCR reaction were used as templates for sequence- and
512 ligation-independent cloning into antibody expression vectors. Recombinant monoclonal
513 antibodies and Fabs were produced and purified as previously described[8].

514

515 **Cryo-EM sample preparation**

516 Expression and purification of SARS-CoV-2 6P stabilized S trimers[37] was conducted as
517 previously described[53]. Purified Fab and S 6P trimer were incubated at a 1.1:1 molar ratio per
518 protomer on ice for 30 minutes prior to deposition on a freshly glow-discharged 300 mesh,
519 1.2/1.3 Quantifoil copper grid. Immediately before 3 µl of complex was applied to the grid,
520 fluorinated octyl-malotiside was added to the Fab-S complex to a final detergent concentration of
521 0.02% w/v, resulting in a final complex concentration of 3 mg/ml. Samples were vitrified in
522 100% liquid ethane using a Mark IV Vitrobot after blotting for 3 s with Whatman No. 1 filter
523 paper at 22˚C and 100% humidity.

524

525 **Cryo-EM data collection and processing**

526 Data collection and processing followed a similar workflow to what has been previously
527 described in detail[29]. Briefly, micrographs were collected on a Talos Arctica transmission

528 electron microscope (Thermo Fisher) operating at 200 kV for all Fab-S complexes. Data were
529 collected using SerialEM automated data collection software[54] and movies were recorded with a
530 K3 camera (Gatan). For all datasets, cryo-EM movies were patch motion corrected for beam-
531 induced motion including dose-weighting within cryoSPARC v2.15[55] after binning super
532 resolution movies. The non-dose-weighted images were used to estimate CTF parameters using
533 cryoSPARC implementation of the Patch CTF job. Particles were picked using Blob picker and
534 extracted 4x binned and 2D classified. Class averages corresponding to distinct views with
535 secondary structure features were chosen and ab initio models were generated. 3D classes that
536 showed features of a Fab-S complex were re-extracted, unbinned (0.869 Å/pixel) and
537 homogenously refined with C1 symmetry. Overall resolutions were reported based on gold
538 standard FSC calculations.
539

540 **Cryo-EM Structure Modeling and Refinement**

541 Coordinates for initial complexes were generated by docking individual chains from reference
542 structures into cryo-EM density using UCSF Chimera[56] (S trimer: PDB 6KXL, Fab: PDB 6XCA
543 or 7K8P after trimming CDR3 loops and converting to a polyalanine model). Models were then
544 refined into cryo-EM maps by rigid body and real space refinement in Phenix[57]. If the resolution
545 allowed, partial CDR3 loops were built manually in Coot[58] and then refined using real-space
546 refinement in Phenix.
547

548 **Computational analyses of antibody sequences**

549 Antibody sequences were trimmed based on quality and annotated using Igblastn v.1.14. with
550 IMGT domain delineation system. Annotation was performed systematically using Change-O

551 toolkit v.0.4.540 [59]. Heavy and light chains derived from the same cell were paired, and
552 clonotypes were assigned based on their V and J genes using in-house R and Perl scripts (Fig. 2c
553 and f, Extended data Fig. 3d, Extended data Fig. 4b). All scripts and the data used to process
554 antibody sequences are publicly available on GitHub (https://github.com/stratust/igpipeline).
555
556 The frequency distributions of human V genes in anti-SARS-CoV-2 antibodies from this study
557 was compared to 131,284,220 IgH and IgL sequences generated by [60] and downloaded from
558 cAb-Rep [61], a database of human shared BCR clonotypes available at https://cab-
559 rep.c2b2.columbia.edu/. Based on the 97 distinct V genes that make up the 4186 analyzed
560 sequences from Ig repertoire of the 14 participants present in this study, we selected the IgH and
561 IgL sequences from the database that are partially coded by the same V genes and counted them
562 according to the constant region. The frequencies shown in (Fig 2e and Extended Data Fig 4a)
563 are relative to the source and isotype analyzed. We used the two-sided binomial test to check
564 whether the number of sequences belonging to a specific IgHV or IgLV gene in the repertoire is
565 different according to the frequency of the same IgV gene in the database. Adjusted p-values
566 were calculated using the false discovery rate (FDR) correction. Significant differences are
567 denoted with stars.
568
569 Nucleotide somatic hypermutation and CDR3 length were determined using in-house R and Perl
570 scripts. For somatic hypermutations, IGHV and IGLV nucleotide sequences were aligned against
571 their closest germlines using Igblastn and the number of differences were considered nucleotide
572 mutations. The average mutations for V genes were calculated by dividing the sum of all
573 nucleotide mutations across all participants by the number of sequences used for the analysis. To

574 calculate the GRAVY scores of hydrophobicity[62] we used Guy H.R. Hydrophobicity scale based
575 on free energy of transfer (kcal/mole)[63] implemented by the R package Peptides (the
576 Comprehensive R Archive Network repository; https://journal.r-project.org/archive/2015/RJ-
577 2015-001/RJ-2015-001.pdf). We used 1405 heavy chain CDR3 amino acid sequences from this
578 study and 22,654,256 IGH CDR3 sequences from the public database of memory B cell receptor
579 sequences[64]. The two-tailed Wilcoxon nonparametric test was used to test whether there is a
580 difference in hydrophobicity distribution.
581
582 **Data availability statement:** Data are provided in Extended Data Tables 1-7. The raw
583 sequencing data and computer scripts associated with Fig. 2 have been deposited at Github
584 (https://github.com/stratust/igpipeline). This study also uses data from "A Public Database of
585 Memory and Naive B-Cell Receptor Sequences" [64], PDB (6VYB and 6NB6) and from "High
586 frequency of shared clonotypes in human B cell receptor repertoires" [60]. Cryo-EM maps
587 associated with data reported in this manuscript will be deposited in the Electron Microscopy
588 Data Bank (EMDB: https://www.ebi.ac.uk/pdbe/emdb/) under accession codes EMD-23393
589 (C601-S), EMD-23394 (C603-S), EMD-23395 (C643-S), EMD-23396 (C663-S), EMD-23397
590 (C666-S), EMD-23398 (C669-S), and EMD-23399 (C670-S).
591
592 **Data presentation**
593 Figures were arranged in Adobe Illustrator 2020.
594
595 **Competing interests:** The Rockefeller University has filed a provisional patent application in
596 connection with this work on which Z.W. and M.C.N. are inventors (US patent 63/199, 676).
597

598 **Code availability statement:** Computer code to process the antibody sequences is available at
599 GitHub (https://github.com/stratust/igpipeline).
600
601 **Acknowledgements:** We thank all study participants who devoted time to our research; Drs.
602 Barry Coller and Sarah Schlesinger, the Rockefeller University Hospital Clinical Research
603 Support Office and nursing staff; Charles M. Rice and all members of the M.C.N. laboratory for
604 helpful discussions and Maša Jankovic for laboratory support; and Dr. Jost Vielmetter and the
605 Protein Expression Center in the Beckman Institute at Caltech for expression assistance. Electron
606 microscopy was performed in the Caltech Beckman Institute Resource Center for Transmission
607 Electron Microscopy and we thank Drs. Songye Chen and Andrey Malyutin for technical
608 assistance. This work was supported by NIH grant P01-AI138398-S1 (M.C.N. and P.J.B.) and
609 2U19AI111825 (M.C.N.); the Caltech Merkin Institute for Translational Research and P50
610 AI150464-13 (P.J.B.), a George Mason University Fast Grant (P.J.B.); R37-AI64003 to P.D.B.;
611 R01AI78788 to T.H.; We thank Dr. Jost Vielmetter and the Protein Expression Center in the
612 Beckman Institute at Caltech for expression assistance C.O.B. is supported by the HHMI Hanna
613 Gray and Burroughs Wellcome PDEP fellowships. C.G. was supported by the Robert S. Wennett
614 Post-Doctoral Fellowship, in part by the National Center for Advancing Translational Sciences
615 (National Institutes of Health Clinical and Translational Science Award program, grant UL1
616 TR001866), and by the Shapiro-Silverberg Fund for the Advancement of Translational Research.
617 P.D.B. and M.C.N. are Howard Hughes Medical Institute Investigators.
618
619 **Author Contributions:**

620 P.D.B., P.J.B., R.C., T.H., M.C.N, Z.W., F.S., Y.W. F.M. C.O.B, S.F., D.S.B., M.Cipolla.
621 conceived, designed and analyzed the experiments. M.Caskey, C.G., J.A. L, K.W. D.S.B.
622 designed clinical protocols Z.W., F.S., Y.W. F.M. C.O.B, S.F., D.S.B., M.Cipolla, J.D.S. A.G.
623 Z.Y., M.E.A., K.E.H. carried out experiments. C.G., M.Caskey, K.W. D., R.A.C., A.H., K.G.M.
624 recruited participants and executed clinical protocols. I.S., R.P, J.D., J.X. and C.U.O. processed
625 clinical samples. T.Y.O. and V.R. performed bioinformatic analysis. R.C. P.D.B., P.J.B., T.H.,
626 and M.C.N. wrote the manuscript with input from all co-authors.
627

628 **Extended Data Fig. 1. Plasma antibodies against SARS-CoV-2. a–f**, Results of ELISAs
629 measuring plasma reactivity to S (**a**,**c,e**) and RBD protein (**b,d,f**) of 20 vaccinees (grey curves)
630 and 8 controls (black curves). **a**, Anti-S IgG. **b**, Anti-RBD IgG. **c**, Anti-S IgM. **d**, Anti-RBD
631 IgM. **e**, Anti-S IgA. **f**, Anti-RBD IgA. Left, optical density at 450 nm (OD 450 nm) for the
632 indicated reciprocal plasma dilutions. Right, normalized area under the curve (AUC) values for
633 the 8 controls and 20 vaccinees. Horizontal bars indicate geometric mean. Statistical significance
634 was determined using the two-tailed Mann–Whitney U-test. Average of two or more
635 experiments. **g-i,** Correlations of plasma antibodies measurements. **g,** Normalized AUC for IgG
636 anti-S (X axis) plotted against normalized AUC for IgG anti-RBD (Y axis). **h,** Normalized AUC
637 for IgM anti-S (X axis) plotted against normalized AUC for IgM anti-RBD (Y axis). **i,**
638 Normalized AUC for IgA anti-S (X axis) plotted against normalized AUC for IgA anti-RBD (Y
639 axis). The *r* and *p* values in **g-i** were determined with the two-tailed Spearman's correlation test.
640 Moderna vaccinees are in black and Pfizer-BioNTech in red. **j-l,** Results of ELISAs measuring
641 plasma reactivity to RBD in convalescent volunteers 1.3 and 6.2 months after infection[7,8] and in
642 20 vaccinees, who received the Moderna vaccine (black dots) and Pfizer-BioNTech vaccine (red
643 dots). **j,** Anti-RBD IgG. **k,** Anti-RBD IgM. **l,** Anti-RBD IgA. The normalized area under the
644 curve (AUC) values are shown. Positive and negative controls were included for validation. Red
645 horizontal bars and indicated values represent geometric mean. Statistical significance was
646 determined using two-tailed Mann–Whitney U-test or Wilcoxon matched-pairs signed rank test.
647

648 **Extended Data Fig. 2: Plasma neutralizing activity. a**, Anti-S IgM AUC (Y axis) plotted
649 against NT_{50} (X axis) r=0.12, p<0.62. **b,** Anti-S IgA AUC (Y axis) plotted against NT_{50} (X axis)
650 r=0.79, p<0.0001. **c**, Anti-RBD IgM AUC (Y axis) plotted against NT50 (X axis) r=-0.079

651 p=0.74. **d**, Anti-RBD IgA AUC (Y axis) plotted against NT50 (X axis) r=0.69 p=0.0008. **e**, NT_{50}
652 (Y axis) plotted against time between last dose and blood draw (X axis) r=-0.63 p=0.0032. **f**,
653 NT_{50} (Y axis) plotted against time between doses (X axis) r=0.03 p=0.89. **g**, Anti-RBD IgG AUC
654 (Y axis) plotted against time between last dose and blood draw (X axis) r=-0.57 p=0.0084. **h**,
655 Anti-S IgG AUC (Y axis) plotted against time between last dose and blood draw (X axis) r=-0.59
656 p=0.0064. **i**, Age (Y axis) plotted against NT_{50} (X axis) r=-0.06 p=0.82. The r and p values were
657 determined by two-tailed Spearman's. Moderna vaccinees in black and Pfizer-BioNTech in red.
658 **j**, NT50 values for vaccinee plasma (n=15) neutralization of pseudotyped viruses with WT and
659 the indicated RBD-mutant SARS-CoV-2 S proteins; p-values determined using one tailed t-test.
660
661 **Extended Data Fig. 3: Flow cytometry. a,** Gating strategy used for cell sorting. Gating was on
662 singlets that were CD20+ and CD3-CD8-CD14-CD16-OVA-. Sorted cells were RBD-PE+ and
663 RBD-AF647+. **b,** Flow cytometry showing the percentage of RBD-double positive memory B
664 cells from a pre-COVID-19 control (HD) and 15 vaccinees, who received the Moderna vaccine
665 are shown in black and Pfizer-BioNTech vaccine recipients are in red. **c**, the percentage of RBD-
666 binding memory B cells in vaccinees (Y axis) plotted against time between first dose and blood
667 draw (X axis) r=0.40 p=0.087 (left panel), and between last dose and blood draw (X axis) r=0.33
668 p=0.17 (right panel). Moderna vaccinees in black and Pfizer-BioNTech in red. The r and p values
669 for correlations were determined by two-tailed Spearman's. **d,** Pie charts show the distribution of
670 antibody sequences from 10 individuals in **b.** The number in the inner circle indicates the number
671 of sequences analyzed. Pie slice size is proportional to the number of clonally related sequences.
672 The black outline indicates the frequency of clonally expanded sequences. The r and p values for
673 correlations in **c** were determined by the two-tailed Spearman correlation test.

674

675 **Extended Data Fig. 4: Frequency distributions of human VL genes.**

676 Graph shows relative abundance of human IGVK (left) and IgVL (right) genes of Sequence Read
677 Archive accession SRP010970 (orange)[65], and vaccinees (blue). Two-sided binomial tests with
678 unequal variance were used to compare the frequency distributions., significant differences are
679 denoted with stars (* $p < 0.05$, ** $p < 0.01$, *** $p < 0.001$, **** = $p < 0.0001$). **b.** Sequences
680 from 14 individuals (Extended Data Table 3) with clonal relationships**.** Interconnecting lines
681 indicate the relationship between antibodies that share V and J gene segment sequences at both
682 IGH and IGL. Purple, green and grey lines connect related clones, clones and singles, and singles
683 to each other, respectively.

684

685 **Extended Data Fig. 5: Antibody somatic hypermutation, and CDR3 length. a,** Number of
686 somatic nucleotide mutations in both the IGVH and IGVL in 14 participants (left). Individuals
687 who received the Moderna vaccine are shown in black and Pfizer-BioNTech vaccine recipients
688 in red. For each individual, the number of the amino acid length of the CDR3s at the IGVH and
689 IGVL is shown (right). The horizontal bars indicate the mean. The number of antibody
690 sequences (IGVH and IGVL) evaluated for each participant are n=68 (MOD1), n=45 (MOD2),
691 n=117 (MOD3), n=123 (MOD4), n=110 (MOD6), n=109 (MOD7), n=144 (MOD8), n=102
692 (MOD9), n=132 (PFZ10), n=109 (MOD11), n=91 (PFZ12), n=78 (C001), n=66 (C003), and
693 n=115 (C004). **b,** Distribution of the hydrophobicity GRAVY scores at the IGH CDR3 compared
694 to a public database (see Methods for statistical analysis). The box limits are at the lower and
695 upper quartiles, the center line indicates the median, the whiskers are 1.5× interquartile range and

696 the dots represent outliers. Statistical significance was determined using two-tailed Wilcoxon
697 matched-pairs signed rank test (**** = $p < 0.0001$).
698
699 **Extended Data Fig. 6: Monoclonal antibody ELISAs. a,** Graphs show anti-SARS-CoV-2
700 RBD antibody reactivity. ELISA EC50 values for all antibodies isolated from COVID-19
701 convalescent individuals assayed at 1.3 and 6.2 months after infection[7,8] and 127 selected
702 monoclonal antibodies isolated from 4 Moderna vaccinees (black dots) and 4 Pfizer-BioNTech
703 vaccinees (red dots) measured at 8 weeks after the boost. Red horizontal bars and indicated
704 values represent geometric mean. Statistical significance was determined using two-tailed
705 Mann–Whitney U-test. **b-c**, Graphs show ELISA titration curves for 86 monoclonal antibodies
706 isolated from Moderna vaccinees (**b**) and 41 monoclonal antibodies isolated from Pfizer-
707 BioNTech vaccinees (**c**). **d-l,** Graphs show ELISA titrations for 84 antibodies isolated from
708 Moderna vaccinees against the indicated RBD variants. Isotype control and low-binding
709 antibodies are indicated in colors. C661 is a non-binding antibody. Data are representative of two
710 independent experiments. **m,** Relative change in EC50 values for the indicated RBD variants
711 over wt RBD of 84 antibodies isolated from Moderna vaccinees. Red horizontal bars represent
712 geometric mean. **n,** a heat map summary of EC_{50} values for binding to wild type RBD and the
713 indicated mutant RBDs for 17 top neutralizing antibodies.
714
715 **Extended Data Fig. 7: Neutralizing activity of monoclonal antibodies in clinical**
716 **development against SARS-CoV-2 variants. a,** Results of a SARS-CoV-2 pseudovirus
717 neutralization assay. IC_{50} values for 6 different monoclonal antibodies, alone or in their clinically
718 designated combinations, for neutralization of wild type and the indicated mutant SARS-CoV-2

719 pseudotyped viruses. Antibodies with IC_{50} values above 1000 ng/ml were plotted at 1000 ng/ml.
720 Data are the mean of 2 independent experiments. Color gradient indicates IC_{50} values ranging
721 from 0 (white) to 1000 ng/ml (red). The combination of REGN 10987 and 10933 (casirivimab
722 and imdevimab, respectively)[13,66,67] has been granted emergency use authorization by the U.S.
723 FDA, the combination of COV2-2196 and COV2-2130 (licensed to Astra Zeneca as
724 AZD7442)[26], and the combination of C135 and C144 (The Rockefeller University)[8] are currently
725 in clinical trials (NCT04507256 and NCT04700163, respectively).
726
727 **Extended Data Fig. 8: Local resolution estimates of Fab-S cryo-EM reconstructions. a-g,**
728 Local resolution maps calculated using cryoSPARC for (**a**) C669-S, (**b**) C643-S, (**c**) C603-S, (**d**)
729 C601-S, (**e**) C666-S, (**f**) C663-S, and (**g**) C670-S complexes. Close-up views for Fab-RBD
730 interfaces are highlighted for (**a**) C669 and (**b**) C643. **h,** Gold-standard Fourier shell correlation
731 curves for Fab-S complexes. The 0.5 and 0.143 cutoffs are indicated by dashed lines.
732

733

734 **Supplementary Guide**

735 **Supplementary Table 1: Individual vaccinee characteristics**

736 **Supplementary Table 2: Neutralization of WT/KEN pseudovirus by convalescent plasma**

737 **Supplementary Table 3: Antibody sequences from vaccinees is provided as a separate Excel**

738 **file**

739 **Supplementary Table 4: CDR3 alignment of highly identical clonal sequences**

740 **Supplementary Table 5: Sequences, half maximal effective concentrations (EC50s) and**

741 **inhibitory concentrations (IC50s) of the cloned monoclonal antibodies is provided as a**

742 **separate Excel file**

743 **Supplementary Table 6: Neutralization activity of mAbs against mutant SARS-CoV-2**

744 **pseudoviruses**

745 **Supplementary Table 7: Cryo-EM data collection and processing statistics**

746
747

748 **REFERENCES**

749 1 Gaebler, C. & Nussenzweig, M. C. All eyes on a hurdle race for a SARS-CoV-2 vaccine.
750 *Nature* **586**, 501-502, doi:10.1038/d41586-020-02926-w (2020).
751 2 Krammer, F. SARS-CoV-2 vaccines in development. *Nature* **586**, 516-527,
752 doi:10.1038/s41586-020-2798-3 (2020).
753 3 Jackson, L. A. *et al.* An mRNA Vaccine against SARS-CoV-2 - Preliminary Report. *N*
754 *Engl J Med* **383**, 1920-1931, doi:10.1056/NEJMoa2022483 (2020).
755 4 Polack, F. P. *et al.* Safety and Efficacy of the BNT162b2 mRNA Covid-19 Vaccine. *N*
756 *Engl J Med* **383**, 2603-2615, doi:10.1056/NEJMoa2034577 (2020).
757 5 Walsh, E. E. *et al.* Safety and Immunogenicity of Two RNA-Based Covid-19 Vaccine
758 Candidates. *N Engl J Med* **383**, 2439-2450, doi:10.1056/NEJMoa2027906 (2020).
759 6 Sahin, U. *et al.* COVID-19 vaccine BNT162b1 elicits human antibody and TH1 T cell
760 responses. *Nature* **586**, 594-599, doi:10.1038/s41586-020-2814-7 (2020).
761 7 Gaebler, C. *et al.* Evolution of antibody immunity to SARS-CoV-2. *Nature*,
762 doi:10.1038/s41586-021-03207-w (2021).
763 8 Robbiani, D. F. *et al.* Convergent antibody responses to SARS-CoV-2 in convalescent
764 individuals. *Nature* **584**, 437-442, doi:10.1038/s41586-020-2456-9 (2020).
765 9 Corbett, K. S. *et al.* Evaluation of the mRNA-1273 Vaccine against SARS-CoV-2 in
766 Nonhuman Primates. *N Engl J Med* **383**, 1544-1555, doi:10.1056/NEJMoa2024671
767 (2020).
768 10 Schmidt, F. *et al.* Measuring SARS-CoV-2 neutralizing antibody activity using
769 pseudotyped and chimeric viruses. *J Exp Med* **217**, doi:10.1084/jem.20201181 (2020).
770 11 Widge, A. T. *et al.* Durability of Responses after SARS-CoV-2 mRNA-1273
771 Vaccination. *N Engl J Med* **384**, 80-82, doi:10.1056/NEJMc2032195 (2021).
772 12 Weisblum, Y. *et al.* Escape from neutralizing antibodies by SARS-CoV-2 spike protein
773 variants. *Elife* **9**, doi:10.7554/eLife.61312 (2020).
774 13 Baum, A. *et al.* Antibody cocktail to SARS-CoV-2 spike protein prevents rapid
775 mutational escape seen with individual antibodies. *Science* **369**, 1014-1018,
776 doi:10.1126/science.abd0831 (2020).
777 14 Davies, N. G. *et al.* Estimated transmissibility and severity of novel SARS-CoV-2
778 Variant of Concern 202012/01 in England. *medRxiv*, 2020.2012.2024.20248822,
779 doi:10.1101/2020.12.24.20248822 (2020).
780 15 Greaney, A. J. *et al.* Comprehensive mapping of mutations to the SARS-CoV-2 receptor-
781 binding domain that affect recognition by polyclonal human serum antibodies. *bioRxiv*
782 **588**, 682-635, doi:10.1101/2020.12.31.425021 (2021).
783 16 Greaney, A. J. *et al.* Complete Mapping of Mutations to the SARS-CoV-2 Spike
784 Receptor-Binding Domain that Escape Antibody Recognition. *Cell Host Microbe* **29**, 44-
785 57 e49, doi:10.1016/j.chom.2020.11.007 (2021).
786 17 Japan, N. I. o. I. D. Brief report: New Variant Strain of SARS-CoV-2 Identified in
787 Travelers from Brazil. doi:https://www.niid.go.jp/niid/images/epi/corona/covid19-33-en-
788 210112.pdf (2021).
789 18 Tegally, H. *et al.* Emergence and rapid spread of a new severe acute respiratory
790 syndrome-related coronavirus 2 (SARS-CoV-2) lineage with multiple spike mutations in
791 South Africa. *medRxiv*, 2020.2012.2021.20248640, doi:10.1101/2020.12.21.20248640
792 (2020).

793 19 Lauring, A. S. & Hodcroft, E. B. Genetic Variants of SARS-CoV-2-What Do They
794 Mean? *JAMA*, 1-3, doi:10.1001/jama.2020.27124 (2021).
795 20 Amanna, I. J., Carlson, N. E. & Slifka, M. K. Duration of humoral immunity to common
796 viral and vaccine antigens. *N Engl J Med* **357**, 1903-1915, doi:10.1056/NEJMoa066092
797 (2007).
798 21 Brouwer, P. J. M. *et al.* Potent neutralizing antibodies from COVID-19 patients define
799 multiple targets of vulnerability. *Science* **369**, 643-650, doi:10.1126/science.abc5902
800 (2020).
801 22 Cao, Y. *et al.* Potent Neutralizing Antibodies against SARS-CoV-2 Identified by High-
802 Throughput Single-Cell Sequencing of Convalescent Patients' B Cells. *Cell* **182**, 73-84
803 e16, doi:10.1016/j.cell.2020.05.025 (2020).
804 23 Ju, B. *et al.* Human neutralizing antibodies elicited by SARS-CoV-2 infection. *Nature*
805 **584**, 115-119, doi:10.1038/s41586-020-2380-z (2020).
806 24 Liu, L. *et al.* Potent neutralizing antibodies against multiple epitopes on SARS-CoV-2
807 spike. *Nature* **584**, 450-456, doi:10.1038/s41586-020-2571-7 (2020).
808 25 Rogers, T. F. *et al.* Isolation of potent SARS-CoV-2 neutralizing antibodies and
809 protection from disease in a small animal model. *Science* **369**, 956-963,
810 doi:10.1126/science.abc7520 (2020).
811 26 Zost, S. J. *et al.* Potently neutralizing and protective human antibodies against SARS-
812 CoV-2. *Nature* **584**, 443-449, doi:10.1038/s41586-020-2548-6 (2020).
813 27 Briney, B., Inderbitzin, A., Joyce, C. & Burton, D. R. Commonality despite exceptional
814 diversity in the baseline human antibody repertoire. *Nature* **566**, 393-397,
815 doi:10.1038/s41586-019-0879-y (2019).
816 28 Andreano, E. *et al.* SARS-CoV-2 escape in vitro from a highly neutralizing COVID-19
817 convalescent plasma. *bioRxiv* **5**, 237-236, doi:10.1101/2020.12.28.424451 (2020).
818 29 Barnes, C. O. *et al.* SARS-CoV-2 neutralizing antibody structures inform therapeutic
819 strategies. *Nature* **588**, 682-687, doi:10.1038/s41586-020-2852-1 (2020).
820 30 Barnes, C. O. *et al.* Structures of Human Antibodies Bound to SARS-CoV-2 Spike
821 Reveal Common Epitopes and Recurrent Features of Antibodies. *Cell* **182**, 828-842 e816,
822 doi:10.1016/j.cell.2020.06.025 (2020).
823 31 Thomson, E. C. *et al.* Circulating SARS-CoV-2 spike N439K variants maintain fitness
824 while evading antibody-mediated immunity. *Cell*, 2020.2011.2004.355842,
825 doi:10.1016/j.cell.2021.01.037 (2021).
826 32 Tortorici, M. A. *et al.* Ultrapotent human antibodies protect against SARS-CoV-2
827 challenge via multiple mechanisms. *Science* **370**, 950-957, doi:10.1126/science.abe3354
828 (2020).
829 33 Starr, T. N. *et al.* Prospective mapping of viral mutations that escape antibodies used to
830 treat COVID-19. *Science*, doi:10.1126/science.abf9302 (2021).
831 34 Singer, J., Gifford, R., Cotten, M. & Robertson, D. CoV-GLUE: A Web Application for
832 Tracking SARS-CoV-2 Genomic Variation. *Preprints*,
833 doi:10.20944/preprints202006.0225.v1 (2020).
834 35 Elbe, S. & Buckland-Merrett, G. Data, disease and diplomacy: GISAID's innovative
835 contribution to global health. *Glob Chall* **1**, 33-46, doi:10.1002/gch2.1018 (2017).
836 36 Voloch, C. M. *et al.* Genomic characterization of a novel SARS-CoV-2 lineage from Rio
837 de Janeiro, Brazil. *medRxiv* (2020).

838 37 Hsieh, C. L. *et al.* Structure-based design of prefusion-stabilized SARS-CoV-2 spikes.
839 *Science* **369**, 1501-1505, doi:10.1126/science.abd0826 (2020).
840 38 Ke, Z. *et al.* Structures and distributions of SARS-CoV-2 spike proteins on intact virions.
841 *Nature* **588**, 498-502, doi:10.1038/s41586-020-2665-2 (2020).
842 39 Piccoli, L. *et al.* Mapping Neutralizing and Immunodominant Sites on the SARS-CoV-2
843 Spike Receptor-Binding Domain by Structure-Guided High-Resolution Serology. *Cell*
844 **183**, 1024-1042 e1021, doi:10.1016/j.cell.2020.09.037 (2020).
845 40 Schafer, A. *et al.* Antibody potency, effector function, and combinations in protection
846 and therapy for SARS-CoV-2 infection in vivo. *J Exp Med* **218**,
847 doi:10.1084/jem.20201993 (2021).
848 41 Mendoza, P. *et al.* Combination therapy with anti-HIV-1 antibodies maintains viral
849 suppression. *Nature* **561**, 479-484, doi:10.1038/s41586-018-0531-2 (2018).
850 42 Bar-On, Y. *et al.* Safety and antiviral activity of combination HIV-1 broadly neutralizing
851 antibodies in viremic individuals. *Nat Med* **24**, 1701-1707, doi:10.1038/s41591-018-
852 0186-4 (2018).
853 43 Pinto, D. *et al.* Cross-neutralization of SARS-CoV-2 by a human monoclonal SARS-CoV
854 antibody. *Nature* **583**, 290-295, doi:10.1038/s41586-020-2349-y (2020).
855 44 Rappazzo, C. G. *et al.* An Engineered Antibody with Broad Protective Efficacy in
856 Murine Models of SARS and COVID-19. *bioRxiv*, doi:10.1101/2020.11.17.385500
857 (2020).
858 45 Cele, S. *et al.* Escape of SARS-CoV-2 501Y.V2 variants from neutralization by
859 convalescent plasma. *medRxiv*, 2021.2001.2026.21250224,
860 doi:10.1101/2021.01.26.21250224 (2021).
861 46 Wu, K. *et al.* mRNA-1273 vaccine induces neutralizing antibodies against spike mutants
862 from global SARS-CoV-2 variants. *bioRxiv*, 2021.2001.2025.427948,
863 doi:10.1101/2021.01.25.427948 (2021).
864 47 Xie, X. *et al.* Neutralization of N501Y mutant SARS-CoV-2 by BNT162b2 vaccine-
865 elicited sera. *bioRxiv*, 2021.2001.2007.425740, doi:10.1101/2021.01.07.425740 (2021).
866 48 Wibmer, C. K. *et al.* SARS-CoV-2 501Y.V2 escapes neutralization by South African
867 COVID-19 donor plasma. *bioRxiv*, 2021.2001.2018.427166,
868 doi:10.1101/2021.01.18.427166 (2021).
869 49 Li, Q. *et al.* The Impact of Mutations in SARS-CoV-2 Spike on Viral Infectivity and
870 Antigenicity. *Cell* **182**, 1284-1294 e1289, doi:10.1016/j.cell.2020.07.012 (2020).
871 50 Eguia, R. *et al.* A human coronavirus evolves antigenically to escape antibody immunity.
872 *bioRxiv* **5**, 52-28, doi:10.1101/2020.12.17.423313 (2020).
873 51 Amanat, F. *et al.* A serological assay to detect SARS-CoV-2 seroconversion in humans.
874 *Nat Med* **26**, 1033-1036, doi:10.1038/s41591-020-0913-5 (2020).
875 52 Grifoni, A. *et al.* Targets of T Cell Responses to SARS-CoV-2 Coronavirus in Humans
876 with COVID-19 Disease and Unexposed Individuals. *Cell* **181**, 1489-1501 e1415,
877 doi:10.1016/j.cell.2020.05.015 (2020).
878 53 Cohen, A. A. *et al.* Mosaic nanoparticles elicit cross-reactive immune responses to
879 zoonotic coronaviruses in mice. *Science*, doi:10.1126/science.abf6840 (2021).
880 54 Mastronarde, D. N. Automated electron microscope tomography using robust prediction
881 of specimen movements. *J Struct Biol* **152**, 36-51, doi:10.1016/j.jsb.2005.07.007 (2005).

882 55 Punjani, A., Rubinstein, J. L., Fleet, D. J. & Brubaker, M. A. cryoSPARC: algorithms for
883 rapid unsupervised cryo-EM structure determination. *Nat Methods* **14**, 290-296,
884 doi:10.1038/nmeth.4169 (2017).
885 56 Goddard, T. D. *et al.* UCSF ChimeraX: Meeting modern challenges in visualization and
886 analysis. *Protein Sci* **27**, 14-25, doi:10.1002/pro.3235 (2018).
887 57 Terwilliger, T. C., Adams, P. D., Afonine, P. V. & Sobolev, O. V. A fully automatic
888 method yielding initial models from high-resolution cryo-electron microscopy maps. *Nat*
889 *Methods* **15**, 905-908, doi:10.1038/s41592-018-0173-1 (2018).
890 58 Emsley, P., Lohkamp, B., Scott, W. G. & Cowtan, K. Features and development of Coot.
891 *Acta Crystallogr D Biol Crystallogr* **66**, 486-501, doi:10.1107/S0907444910007493
892 (2010).
893 59 Gupta, N. T. *et al.* Change-O: a toolkit for analyzing large-scale B cell immunoglobulin
894 repertoire sequencing data. *Bioinformatics* **31**, 3356-3358,
895 doi:10.1093/bioinformatics/btv359 (2015).
896 60 Soto, C. *et al.* High frequency of shared clonotypes in human B cell receptor repertoires.
897 *Nature* **566**, 398-402, doi:10.1038/s41586-019-0934-8 (2019).
898 61 Guo, Y., Chen, K., Kwong, P. D., Shapiro, L. & Sheng, Z. cAb-Rep: A Database of
899 Curated Antibody Repertoires for Exploring Antibody Diversity and Predicting Antibody
900 Prevalence. *Front Immunol* **10**, 2365, doi:10.3389/fimmu.2019.02365 (2019).
901 62 Kyte, J. & Doolittle, R. F. A simple method for displaying the hydropathic character of a
902 protein. *J Mol Biol* **157**, 105-132, doi:10.1016/0022-2836(82)90515-0 (1982).
903 63 Guy, H. R. Amino acid side-chain partition energies and distribution of residues in
904 soluble proteins. *Biophys J* **47**, 61-70, doi:10.1016/S0006-3495(85)83877-7 (1985).
905 64 DeWitt, W. S. *et al.* A Public Database of Memory and Naive B-Cell Receptor
906 Sequences. *PLoS One* **11**, e0160853, doi:10.1371/journal.pone.0160853 (2016).
907 65 Rubelt, F. *et al.* Onset of immune senescence defined by unbiased pyrosequencing of
908 human immunoglobulin mRNA repertoires. *PLoS One* **7**, e49774,
909 doi:10.1371/journal.pone.0049774 (2012).
910 66 Baum, A. *et al.* REGN-COV2 antibodies prevent and treat SARS-CoV-2 infection in
911 rhesus macaques and hamsters. *Science* **370**, 1110-1115, doi:10.1126/science.abe2402
912 (2020).
913 67 Weinreich, D. M. *et al.* REGN-COV2, a Neutralizing Antibody Cocktail, in Outpatients
914 with Covid-19. *N Engl J Med* **384**, 238-251, doi:10.1056/NEJMoa2035002 (2021).
915

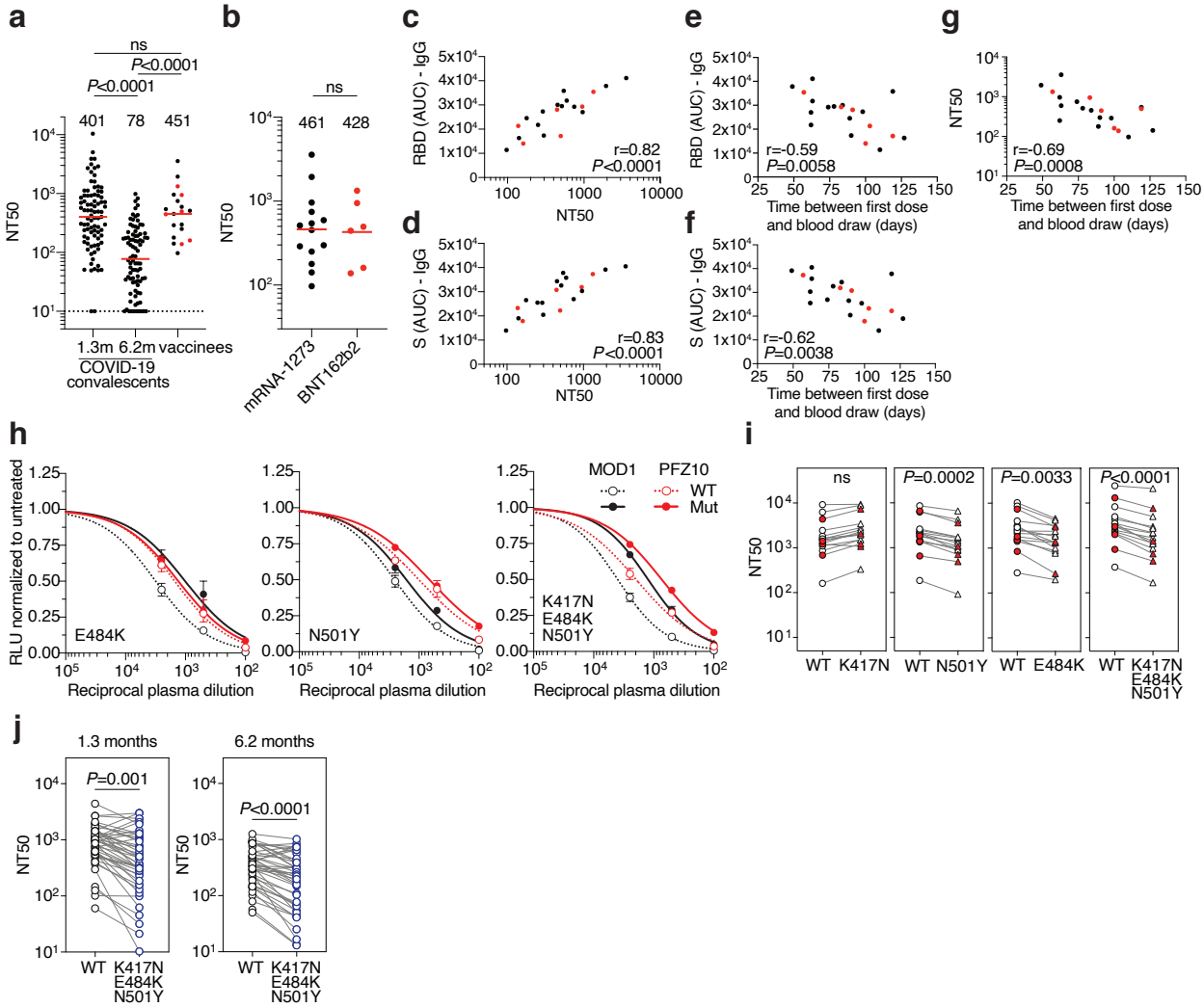
a
ns
P<0.0001
P<0.0001
401 78 451
NT50
1.3m 6.2m vaccinees
COVID-19 convalescents
b
ns
461 428
NT50
mRNA-1273
BNT162b2
c
RBD (AUC) - IgG
r=0.82
P<0.0001
NT50
d
S (AUC) - IgG
r=0.83
P<0.0001
NT50
e
RBD (AUC) - IgG
r=-0.59
P=0.0058
Time between first dose and blood draw (days)
f
S (AUC) - IgG
r=-0.62
P=0.0038
Time between first dose and blood draw (days)
g
NT50
r=-0.69
P=0.0008
Time between first dose and blood draw (days)
h
RLU normalized to untreated
E484K
N501Y
K417N
E484K
N501Y
MOD1
PFZ10
WT
Mut
Reciprocal plasma dilution
i
ns
P=0.0002
P=0.0033
P<0.0001
NT50
WT K417N
WT N501Y
WT E484K
WT K417N E484K N501Y
j
1.3 months
6.2 months
P=0.001
P<0.0001
NT50
WT K417N E484K N501Y

916

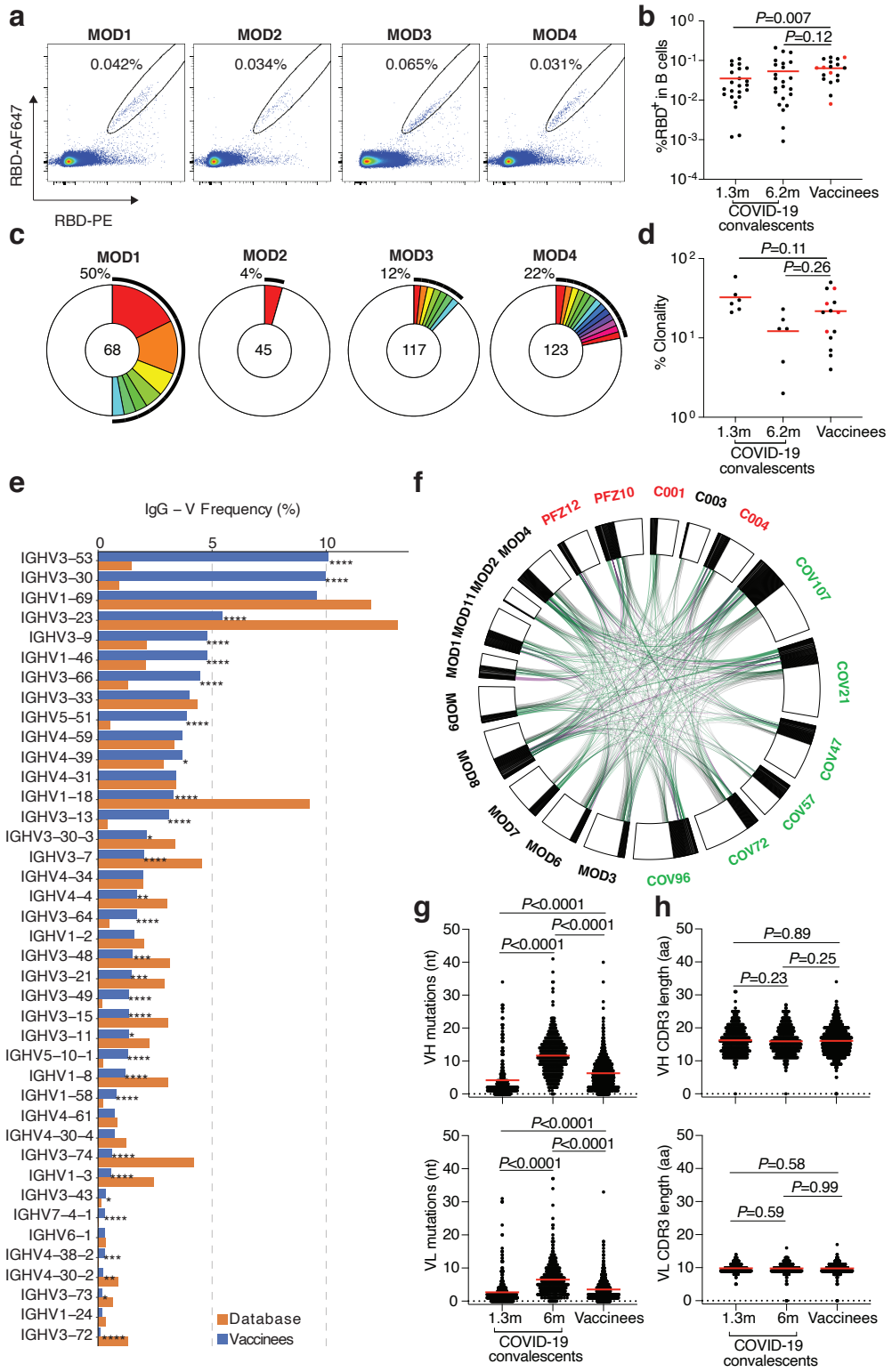
a
MOD1
MOD2
MOD3
MOD4
0.042%
0.034%
0.065%
0.031%
RBD-AF647
RBD-PE
b
P=0.007
P=0.12
%RBD+ in B cells
1.3m
6.2m
Vaccinees
COVID-19 convalescents
c
MOD1
MOD2
MOD3
MOD4
50%
4%
12%
22%
68
45
117
123
d
P=0.11
P=0.26
% Clonality
1.3m
6.2m
Vaccinees
COVID-19 convalescents
e
IgG – V Frequency (%)
IGHV3–53
IGHV3–30
IGHV1–69
IGHV3–23
IGHV3–9
IGHV1–46
IGHV3–66
IGHV3–33
IGHV5–51
IGHV4–59
IGHV4–39
IGHV4–31
IGHV1–18
IGHV3–13
IGHV3–30–3
IGHV3–7
IGHV4–34
IGHV4–4
IGHV3–64
IGHV1–2
IGHV3–48
IGHV3–21
IGHV3–49
IGHV3–15
IGHV3–11
IGHV5–10–1
IGHV1–8
IGHV1–58
IGHV4–61
IGHV4–30–4
IGHV3–74
IGHV1–3
IGHV3–43
IGHV7–4–1
IGHV6–1
IGHV4–38–2
IGHV4–30–2
IGHV3–73
IGHV1–24
IGHV3–72
Database
Vaccinees
f
PFZ12
PFZ10
C001
C003
C004
COV107
COV21
COV47
COV57
COV72
COV96
MOD3
MOD6
MOD7
MOD8
MOD9
MOD1
MOD11
MOD2
MOD4
g
P<0.0001
VH mutations (nt)
VL mutations (nt)
1.3m
6m
Vaccinees
COVID-19 convalescents
h
P=0.89
P=0.25
P=0.23
VH CDR3 length (aa)
P=0.58
P=0.99
P=0.59
VL CDR3 length (aa)

a

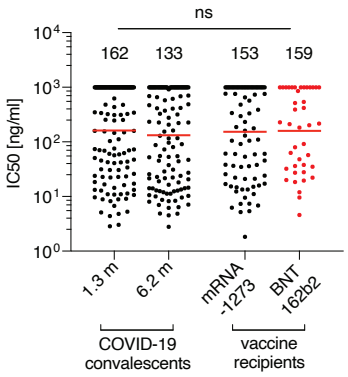

b

		wt	R683G	R346S	K417N	N439K	N440K	Y453F	A475V	S477R	E484K/R683G	Q493R	N501Y	D614G
Class 1	C682	45	29	26	1000	23	43	12	1000	62	110	214	383	28
	C613	20	16	12	273	45	22	47	1000	33	30	236	1000	13
	C663	11	8	8	80	19	14	14	382	17	32	60	1000	12
	C614	5	4	4	1000	4	6	5	32	4	9	7	16	4
	C660	6	4	5	413	9	8	5	8	5	11	8	17	5
Class 1/2	C653	10	7	7	1000	8	9	19	20	10	1000	168	34	8
Class 2	C627	5	3	4	7	3	5	4	4	3	1000	1000	18	4
	C602	14	10	8	5	16	16	13	11	13	1000	58	82	10
	C671	5	3	6	5	5	7	6	6	5	1000	283	28	5
	C643	2	1	1	2	2	2	1	2	2	1000	1	6	2
Class 2/3	C603	14	7	209	5	12	13	12	19	11	1000	7	56	11
	C628	19	12	9	5	257	30	36	16	18	1000	147	1000	14
Class 3	C669	15	17	9	12	1000	1000	20	13	14	24	13	141	17
	C670	14	12	10	8	1000	16	17	12	11	50	15	1000	13
Unclassified	C666	4	2	4	2	3	4	3	7	3	240	4	10	4
	C601	2	1	2	1	2	2	1	2	2	112	3	5	2
	C675	19	12	15	11	17	23	18	38	15	24	14	71	13

c

		K417E	K417N	K417T	N439K	N440H	N440K	L452R	F456S	F456V	N460H	E484D	E484G	E484K	F490S	Q493R	N501H	N501T	N501Y	V503L	G504D	Y508H
Class 1	C682		42	20																		
	C613										16						15		16			
	C663																		71			
	C614	84	13																			
	C660	68	21																			
	C664	82								21												
	C683	26								32												
	C678	11																				
Class 1/2	C653	90				13																
Class 2	C627													37		27						
	C602											14	10	64								
	C671													99								
	C643							41						49								
Class 2/3	C603													67	28							
	C628							58														
Class 3	C669				13		21													23	26	15
	C670				17													16	23		41	
Unclassified	C666								20	77												

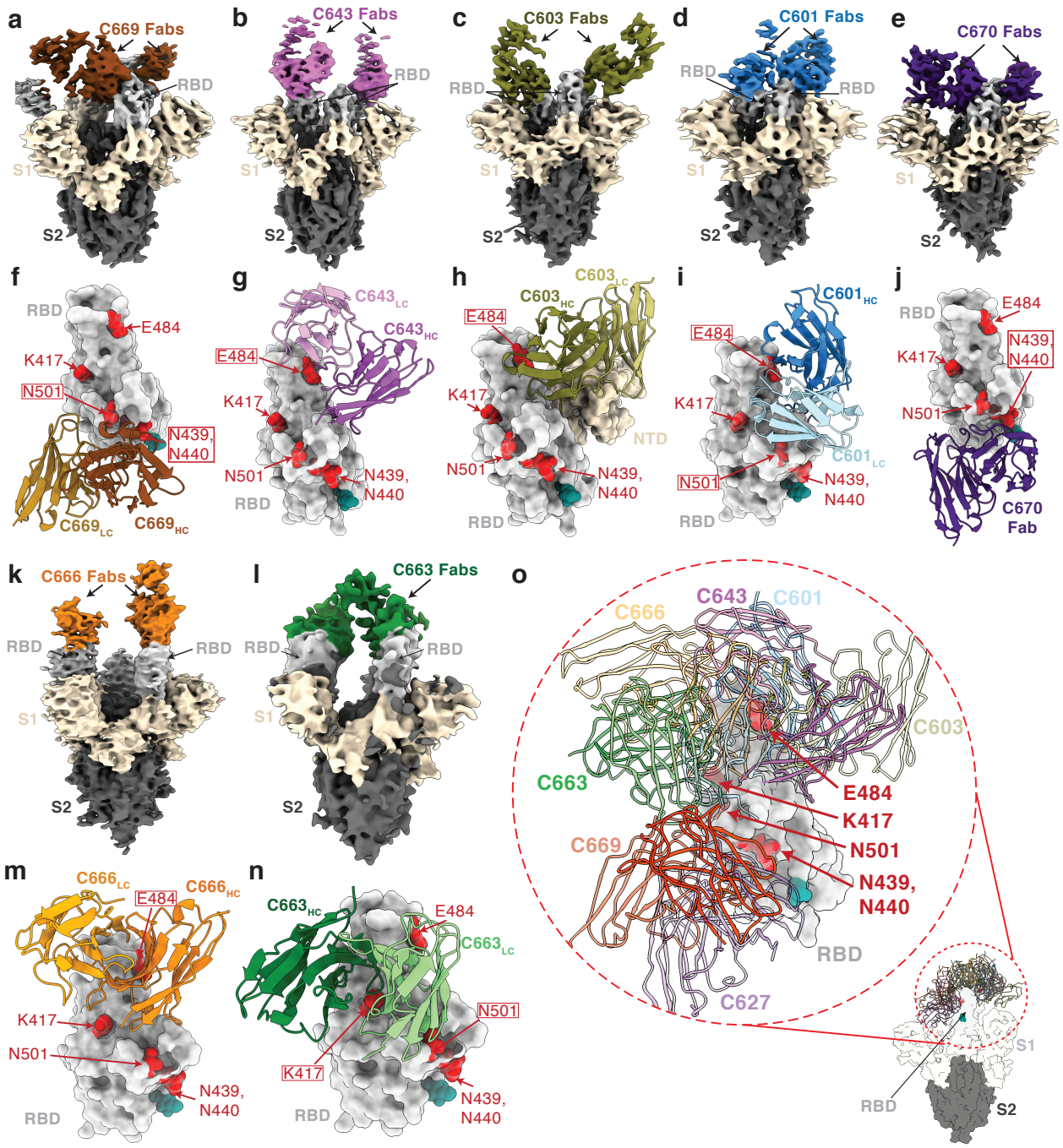
a
C669 Fabs
RBD
S1
S2
b
C643 Fabs
RBD
S1
S2
c
C603 Fabs
RBD
S1
S2
d
C601 Fabs
RBD
RBD
S1
S2
e
C670 Fabs
S1
S2
f
RBD
E484
K417
N501
N439,
N440
C669LC
C669HC
g
C643LC
C643HC
E484
K417
N501
N439,
N440
RBD
h
C603LC
C603HC
E484
K417
NTD
N501
N439,
N440
RBD
i
C601HC
E484
K417
C601LC
N501
N439,
N440
RBD
j
RBD
E484
K417
N439,
N440
N501
C670
Fab
k
C666 Fabs
RBD
RBD
S1
S2
l
C663 Fabs
RBD
RBD
S1
S2
o
C643
C601
C666
C603
C663
E484
K417
N501
C669
N439,
N440
RBD
C627
S1
RBD
S2
m
C666LC
E484
C666HC
K417
N501
N439,
N440
RBD
n
C663HC
E484
C663LC
N501
K417
N439,
N440
RBD

921
922
923

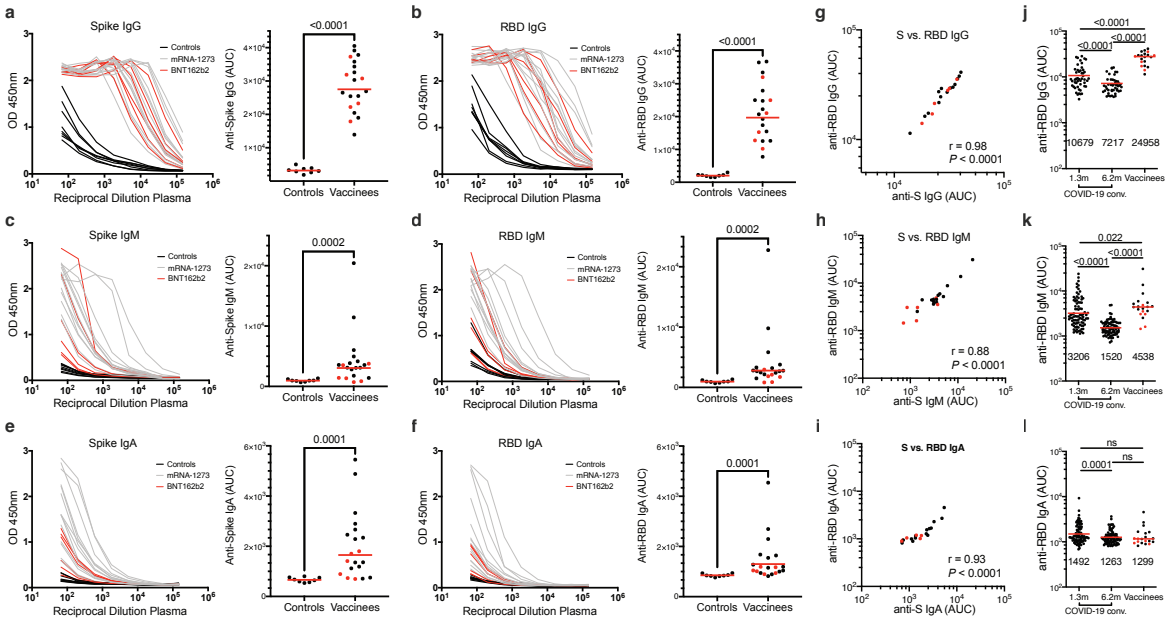
a
Spike IgG
Controls
mRNA-1273
BNT162b2
OD 450nm
Reciprocal Dilution Plasma
Anti-Spike IgG (AUC)
<0.0001
Controls
Vaccinees
b
RBD IgG
Anti-RBD IgG (AUC)
<0.0001
g
S vs. RBD IgG
anti-RBD IgG (AUC)
anti-S IgG (AUC)
r = 0.98
P < 0.0001
j
<0.0001
<0.0001
<0.0001
10679
7217
24958
1.3m
6.2m
Vaccinees
COVID-19 conv.
c
Spike IgM
Anti-Spike IgM (AUC)
0.0002
d
RBD IgM
Anti-RBD IgM (AUC)
0.0002
h
S vs. RBD IgM
anti-RBD IgM (AUC)
anti-S IgM (AUC)
r = 0.88
P < 0.0001
k
0.022
<0.0001
<0.0001
3206
1520
4538
e
Spike IgA
Anti-Spike IgA (AUC)
0.0001
f
RBD IgA
Anti-RBD IgA (AUC)
0.0001
i
S vs. RBD IgA
anti-RBD IgA (AUC)
anti-S IgA (AUC)
r = 0.93
P < 0.0001
l
ns
ns
0.0001
1492
1263
1299

924

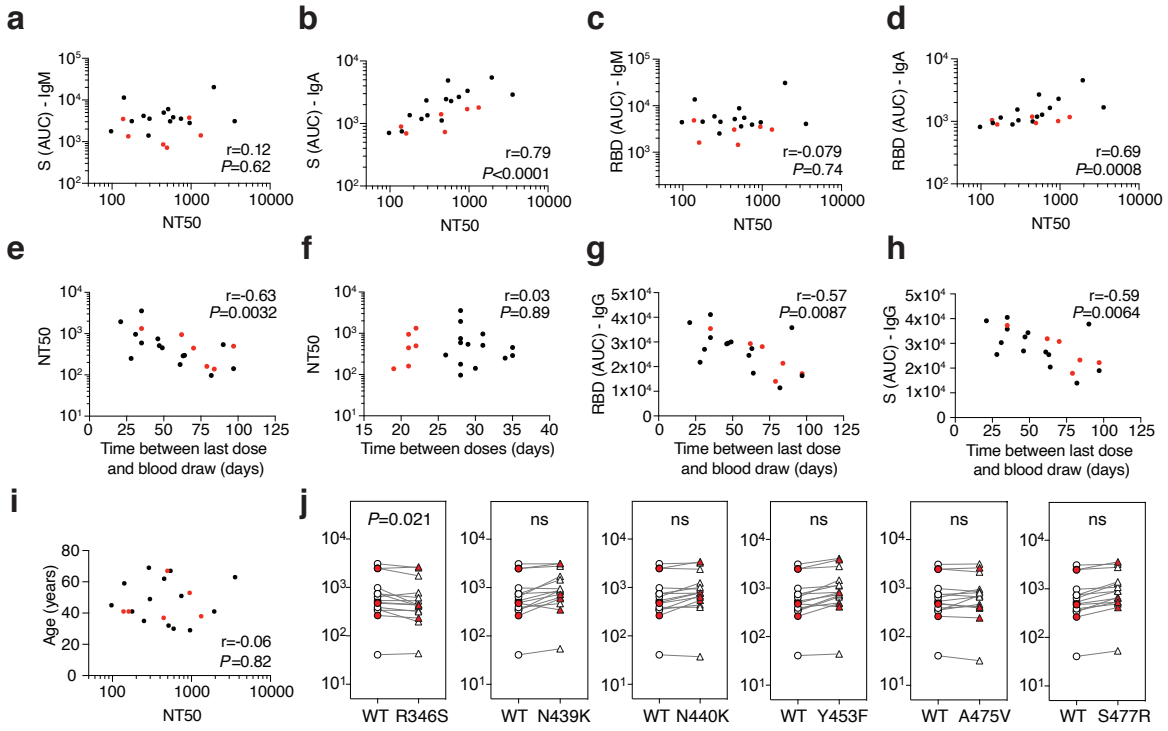
a
S (AUC) - IgM
NT50
r=0.12
P=0.62
b
S (AUC) - IgA
NT50
r=0.79
P<0.0001
c
RBD (AUC) - IgM
NT50
r=-0.079
P=0.74
d
RBD (AUC) - IgA
NT50
r=0.69
P=0.0008
e
NT50
Time between last dose and blood draw (days)
r=-0.63
P=0.0032
f
NT50
Time between doses (days)
r=0.03
P=0.89
g
RBD (AUC) - IgG
Time between last dose and blood draw (days)
r=-0.57
P=0.0087
h
S (AUC) - IgG
Time between last dose and blood draw (days)
r=-0.59
P=0.0064
i
Age (years)
NT50
r=-0.06
P=0.82
j
P=0.021
ns
WT R346S
WT N439K
WT N440K
WT Y453F
WT A475V
WT S477R

925

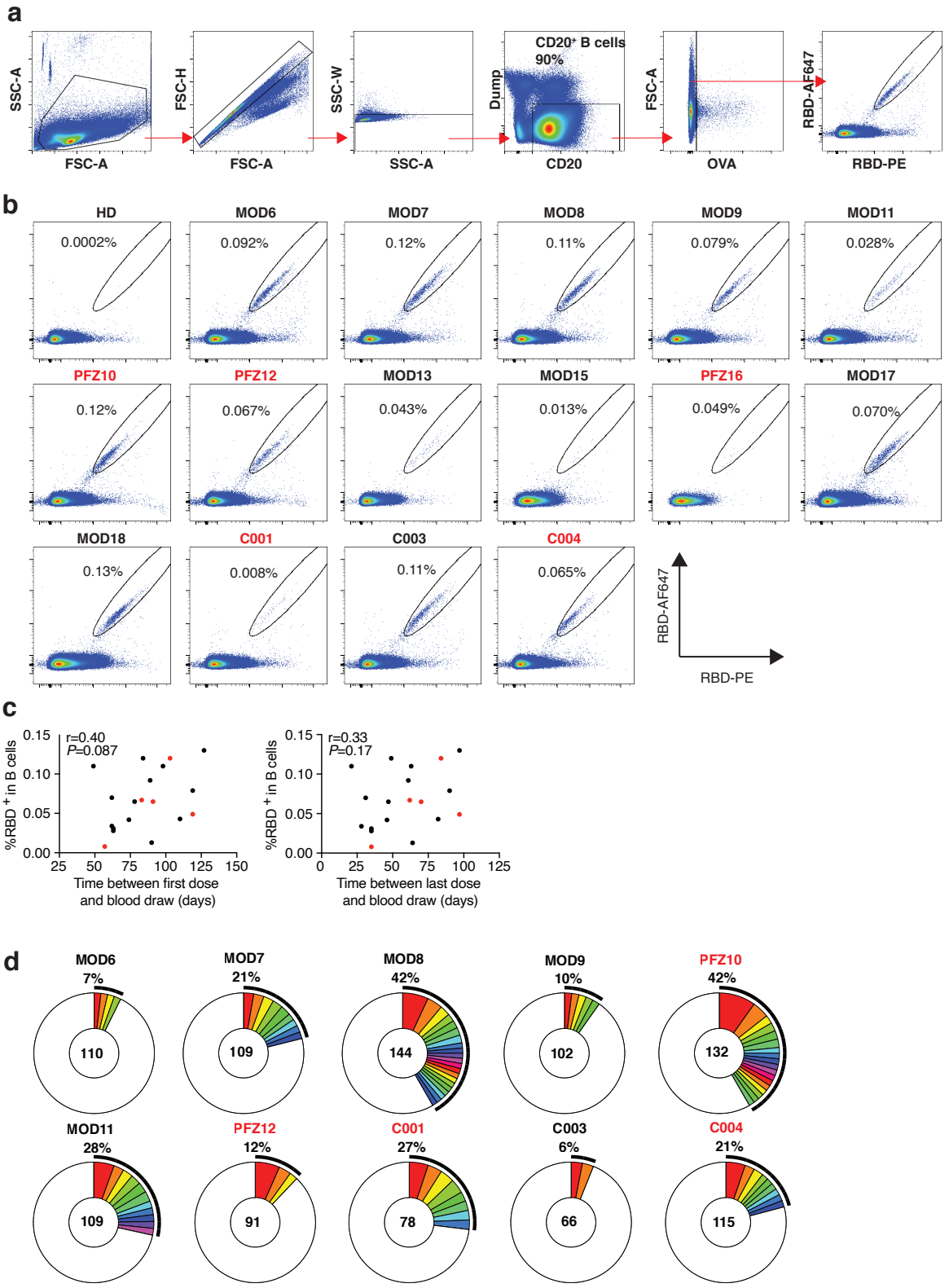
a
SSC-A
FSC-A
FSC-H
FSC-A
SSC-W
SSC-A
Dump
CD20⁺ B cells
90%
CD20
FSC-A
OVA
RBD-AF647
RBD-PE
b
HD
0.0002%
MOD6
0.092%
MOD7
0.12%
MOD8
0.11%
MOD9
0.079%
MOD11
0.028%
PFZ10
0.12%
PFZ12
0.067%
MOD13
0.043%
MOD15
0.013%
PFZ16
0.049%
MOD17
0.070%
MOD18
0.13%
C001
0.008%
C003
0.11%
C004
0.065%
RBD-AF647
RBD-PE
c
r=0.40
P=0.087
%RBD⁺ in B cells
Time between first dose
and blood draw (days)
r=0.33
P=0.17
%RBD⁺ in B cells
Time between last dose
and blood draw (days)
d
MOD6
7%
110
MOD7
21%
109
MOD8
42%
144
MOD9
10%
102
PFZ10
42%
132
MOD11
28%
109
PFZ12
12%
91
C001
27%
78
C003
6%
66
C004
21%
115

926

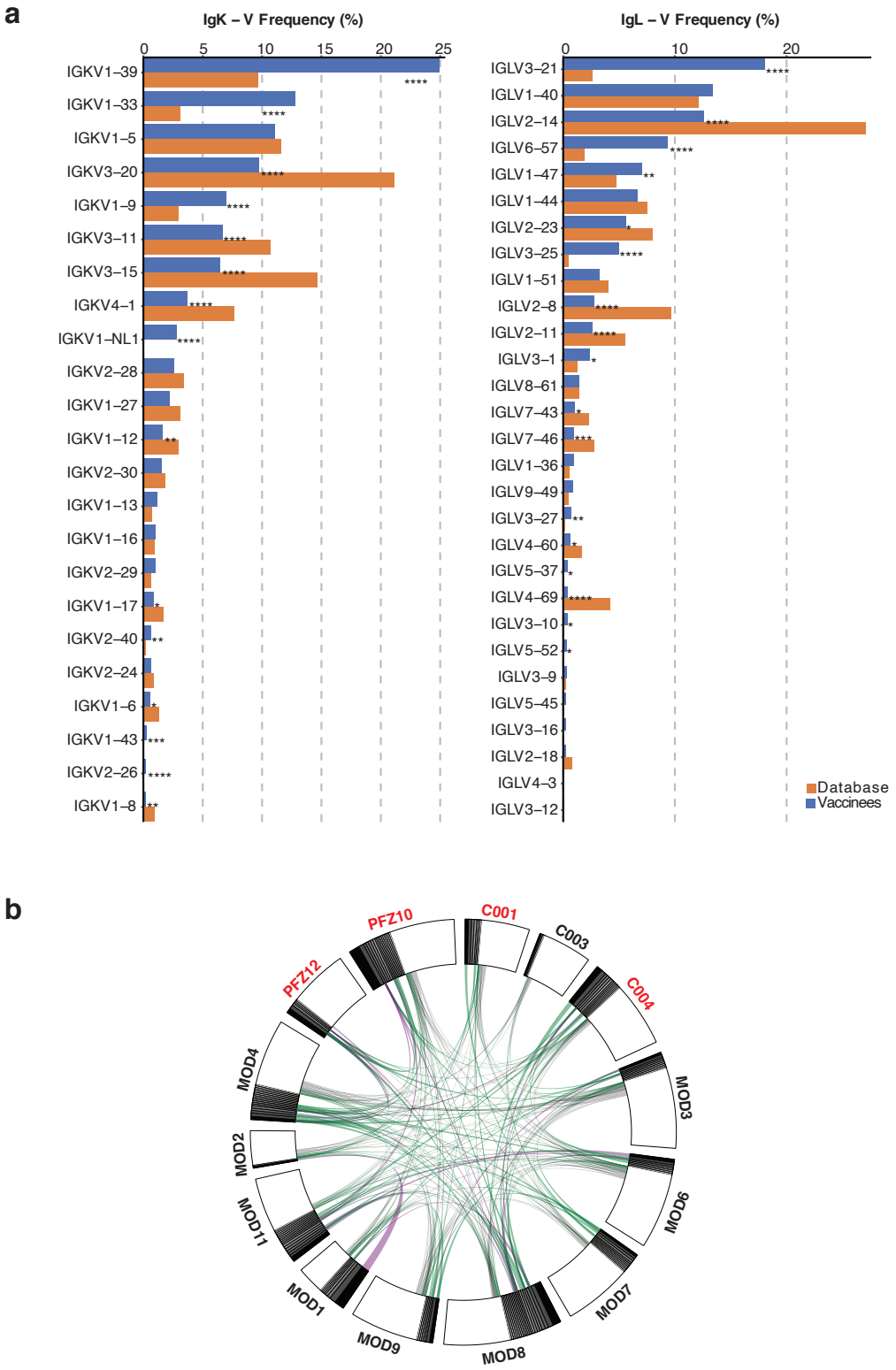
a
IgK – V Frequency (%)
IgL – V Frequency (%)
IGKV1–39
IGKV1–33
IGKV1–5
IGKV3–20
IGKV1–9
IGKV3–11
IGKV3–15
IGKV4–1
IGKV1–NL1
IGKV2–28
IGKV1–27
IGKV1–12
IGKV2–30
IGKV1–13
IGKV1–16
IGKV2–29
IGKV1–17
IGKV2–40
IGKV2–24
IGKV1–6
IGKV1–43
IGKV2–26
IGKV1–8
IGLV3–21
IGLV1–40
IGLV2–14
IGLV6–57
IGLV1–47
IGLV1–44
IGLV2–23
IGLV3–25
IGLV1–51
IGLV2–8
IGLV2–11
IGLV3–1
IGLV8–61
IGLV7–43
IGLV7–46
IGLV1–36
IGLV9–49
IGLV3–27
IGLV4–60
IGLV5–37
IGLV4–69
IGLV3–10
IGLV5–52
IGLV3–9
IGLV5–45
IGLV3–16
IGLV2–18
IGLV4–3
IGLV3–12
Database
Vaccinees
b
PFZ10
C001
C003
C004
PFZ12
MOD4
MOD3
MOD2
MOD6
MOD11
MOD7
MOD1
MOD9
MOD8

927

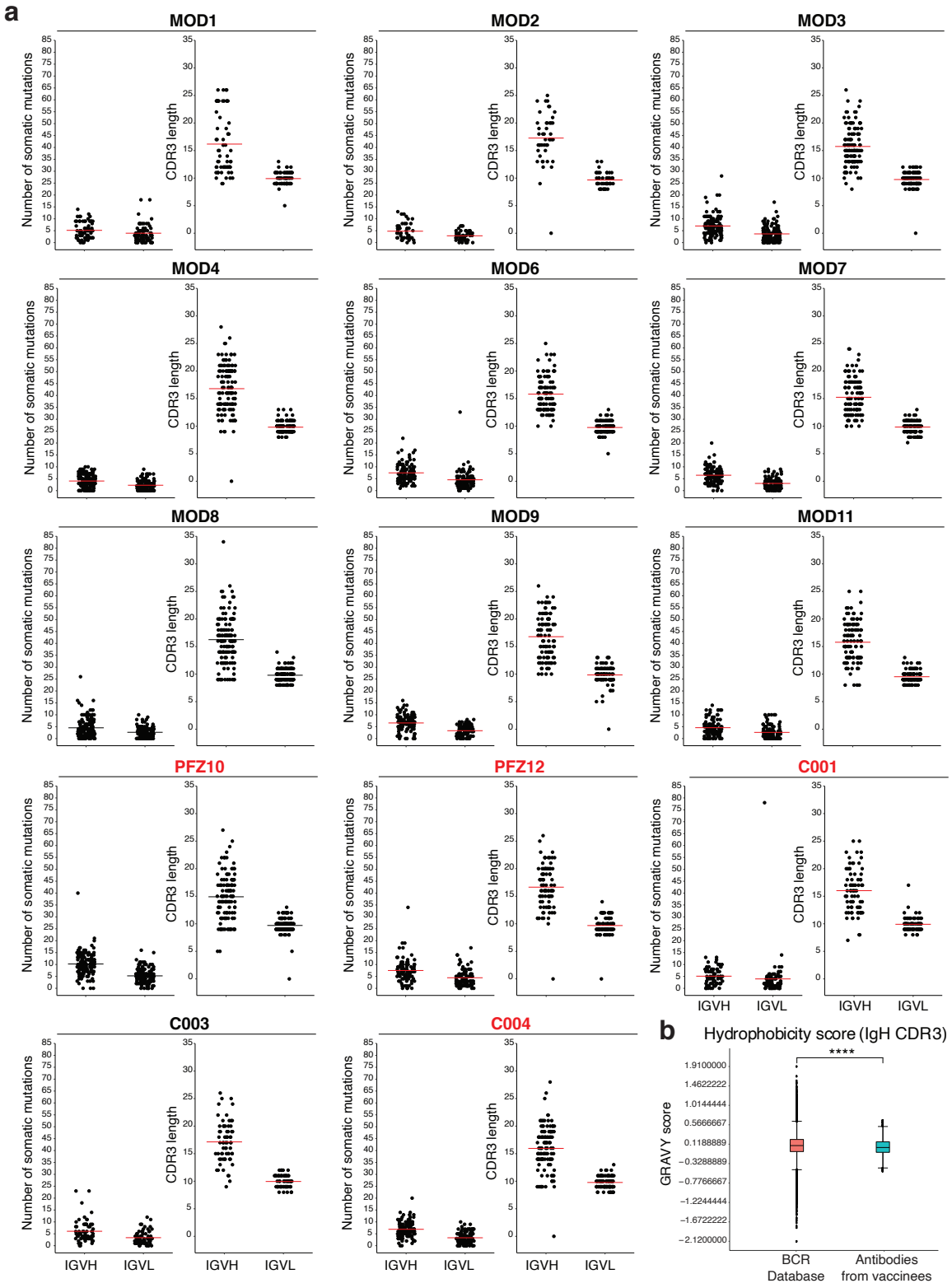
a
MOD1
MOD2
MOD3
MOD4
MOD6
MOD7
MOD8
MOD9
MOD11
PFZ10
PFZ12
C001
C003
C004
Number of somatic mutations
CDR3 length
IGVH
IGVL
b
Hydrophobicity score (IgH CDR3)
****
GRAVY score
BCR Database
Antibodies from vaccinees

928

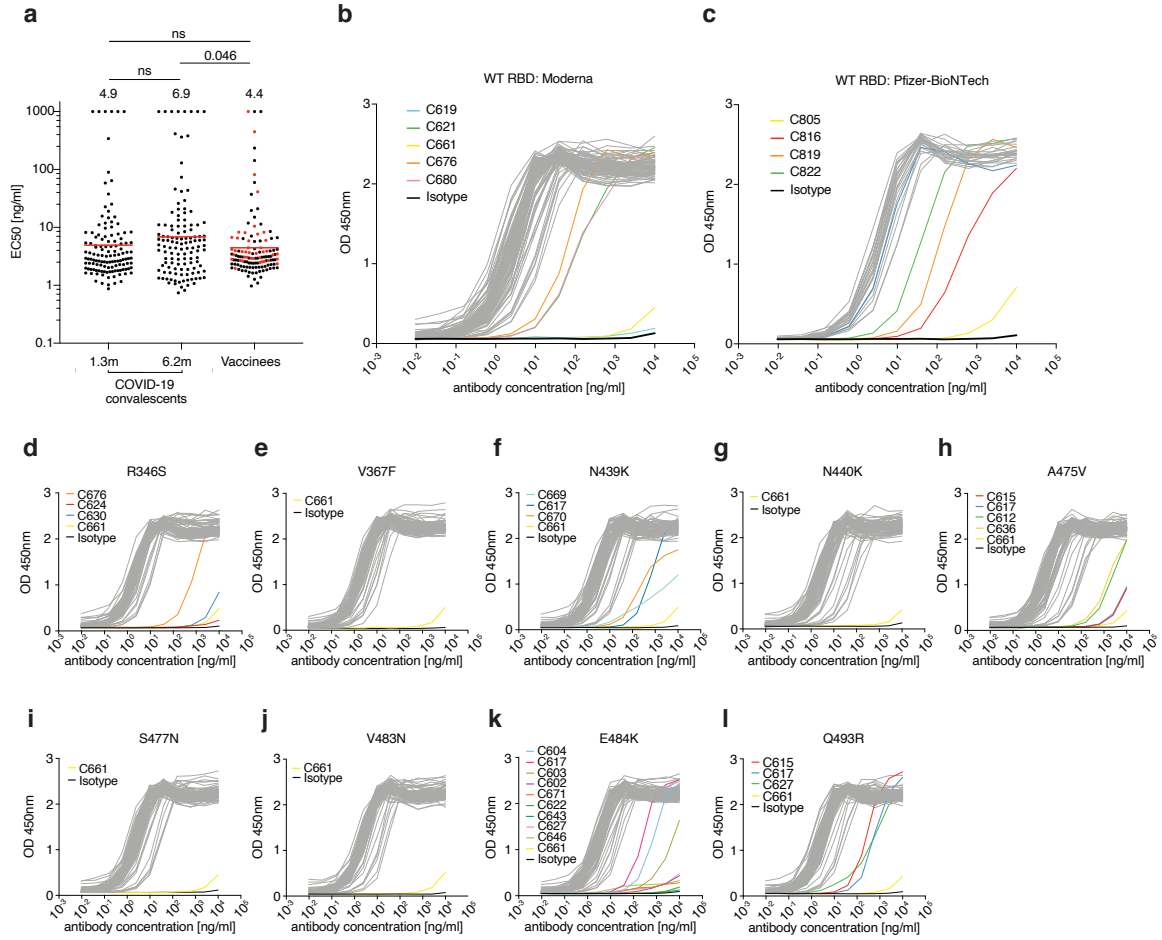

n

		WT	R346S	V367F	N439K	N440K	A475V	S477N	V483A	E484K	Q493R
Class 1	C682	2.4	2.2	2.6	3.6	3.5	35.0	3.3	2.8	3.7	4.1
	C613	2.0	1.9	1.8	3.3	2.5	126.1	2.4	2.3	2.2	4.9
	C663	1.9	1.8	1.7	2.7	2.5	12.6	2.3	2.0	2.4	2.2
	C614	1.4	1.6	1.6	2.0	1.9	2.5	1.8	1.9	1.6	1.8
	C660	2.0	2.0	2.1	2.3	2.7	2.5	2.1	2.2	2.4	2.2
Class 1/2	C653	2.1	2.1	2.1	2.5	2.6	2.2	2.1	2.3	4.0	3.1
Class 2	C627	1.6	1.6	1.8	2.0	2.0	2.1	1.9	1.8	1000	1000
	C602	2.0	1.8	1.9	2.1	2.2	2.2	2.1	3.1	1000	1.9
	C671	2.3	1.7	1.5	2.4	2.4	2.5	2.0	1.8	1000	2.5
	C643	2.1	2.2	2.3	2.0	2.2	1.7	1.8	2.5	1000	1.9
Class 2/3	C603	2.1	1.7	1.7	2.1	2.2	2.3	2.0	1.9	1000	1.9
	C628	2.7	1.9	2.0	4.3	3.2	3.1	2.4	2.4	10.0	3.2
Class 3	C669	2.3	2.1	2.2	950.6	291.8	2.1	2.1	2.2	2.4	2.2
	C670	2.9	2.1	2.3	210.7	2.8	3.0	2.6	2.4	3.3	3.3
Unclassified	C666	1.9	1.7	1.8	2.0	2.1	1.5	1.8	1.9	2.1	1.8
	C601	1.1	1.8	2.1	2.2	2.2	1.9	1.9	2.2	12.1	2.0
	C675	1.3	1.1	1.4	1.8	1.7	3.5	1.4	1.5	1.6	1.4

a

		wt	R683G	K417N	N440K	N501Y	E484K R683G	K417N E484K N501Y R683G
Regeneron	REG10987	8	10	2	765	6	7	2
	REG10933	3	4	17	3	3	36	527
	10987+10933	4	6	3	6	3	9	4
AstraZenca	COV2-2196	3	4	1	2	3	44	16
	COV2-2130	3	5	2	4	3	4	3
	2196+2130	3	5	1	3	2	7	4
RU/BMS	C135	10	18	3	1000	14	7	3
	C144	2	4	1	2	3	1000	1000
	C144+C135	4	6	2	5	4	13	6

IC50 [ng/ml]

932

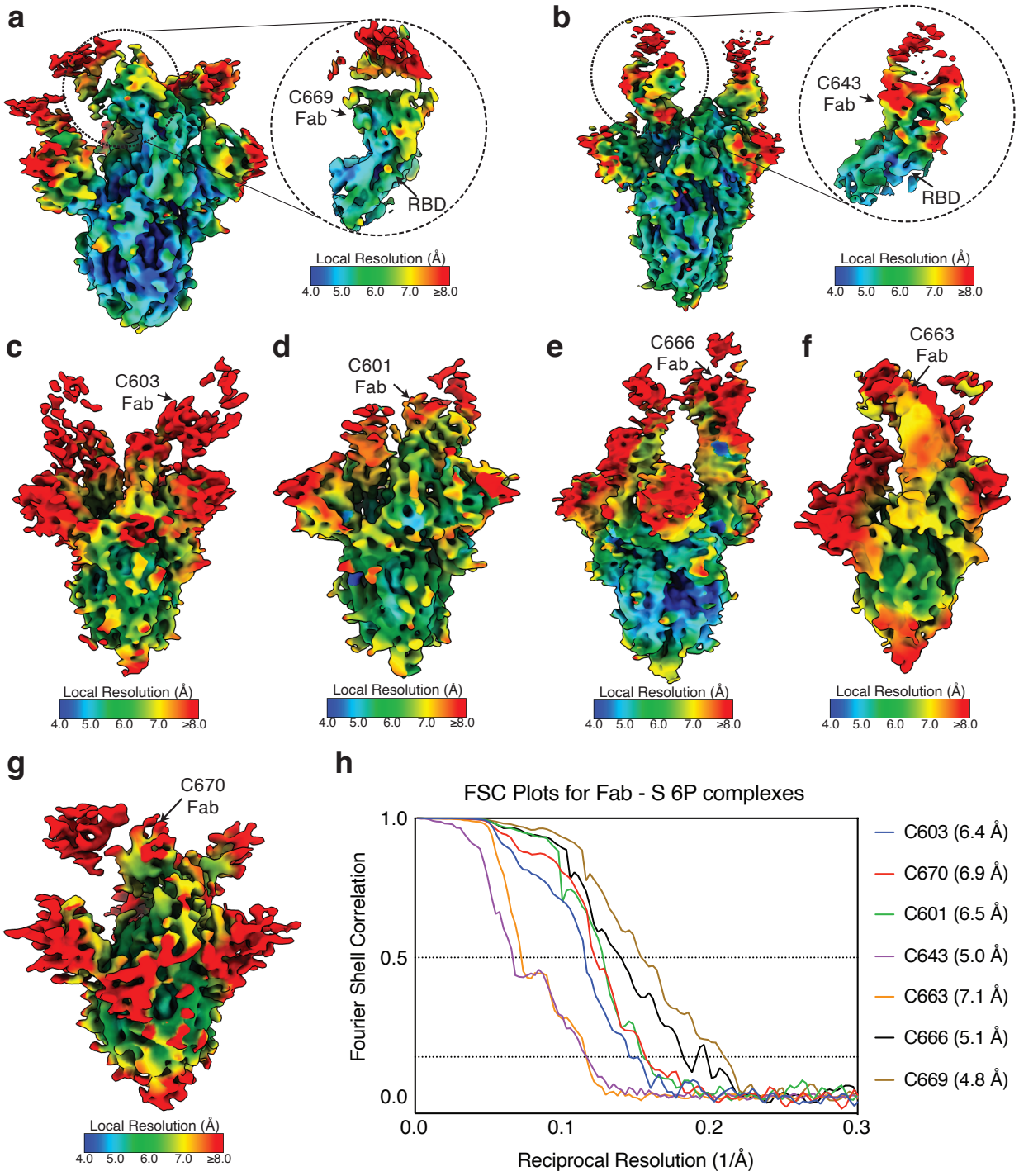
a
C669
Fab
RBD
Local Resolution (Å)
4.0 5.0 6.0 7.0 ≥8.0
b
C643
Fab
RBD
Local Resolution (Å)
4.0 5.0 6.0 7.0 ≥8.0
c
C603
Fab
Local Resolution (Å)
4.0 5.0 6.0 7.0 ≥8.0
d
C601
Fab
Local Resolution (Å)
4.0 5.0 6.0 7.0 ≥8.0
e
C666
Fab
Local Resolution (Å)
4.0 5.0 6.0 7.0 ≥8.0
f
C663
Fab
Local Resolution (Å)
4.0 5.0 6.0 7.0 ≥8.0
g
C670
Fab
Local Resolution (Å)
4.0 5.0 6.0 7.0 ≥8.0
h
FSC Plots for Fab - S 6P complexes
Fourier Shell Correlation
1.0
0.5
0.0
0.0
0.1
0.2
0.3
Reciprocal Resolution (1/Å)
C603 (6.4 Å)
C670 (6.9 Å)
C601 (6.5 Å)
C643 (5.0 Å)
C663 (7.1 Å)
C666 (5.1 Å)
C669 (4.8 Å)

933